Purdue Atmospheric Models and Applications

Wen-Yih Sun[*,**], Wu-Ron Hsu[†,**], Jiun-Dar Chern[‡], Shu-Hua Chen[$,**], Ching-Chi Wu[†], Kate Jr-Shiuan Yang[*], Kaosan Yeh[‡], Michael G. Bosilovich[‡], Patrick A. Haines[¶], Ki-Hong Min[‖], Tae-Jin Oh[*,**], B. T. MacCall[*,**], Ahmet Yildirim[*], Yi-Lin Chang[*], Chiao-Zen Chang[*] and Yi-Chiang Yu[†]

[*] *Purdue University, West Lafayette, Indiana, USA*
[†] *National Taiwan University, Taipei, Taiwan*
[‡] *Goddard Space Fight Center/NASA, Greenbelt, Maryland, USA*
[$] *University of California, Davis, California, USA*
[¶] *Army Research Laboratory, White Sand, New Mexico, USA*
[‖] *Valparaiso University, Valparaiso, Indiana, USA*
[**] *Taiwan Typhoon and Flood Research Institute, Hsin-chu, Taiwan*
wysun@purdue.edu

This article summarizes our research related to geofluid dynamics and numerical modeling. In order to have a better understanding of the motion in the atmosphere, we have been working on various forms of the Navier–Stokes equations, including the linearized and nonlinear systems as well as turbulence parametrization, cumulus parametrization, cloud physics, soil–snow parametrization, atmospheric chemistry, etc. We have also been working on numerical methods in order to solve the equations more accurately. The results show that many weather systems in the initial/growing stage can be qualitatively described by the linearized equations; on the other hand, many developed weather phenomena can be quantitatively reproduced by the nonlinear Purdue Regional Climate Model, when the observational data or reanalysis is used as the initial and lateral boundary conditions. The model can also reveal the detailed structure and physics involved, which sometimes can be misinterpreted by meteorologists according to the incomplete observations. However, it is also noted that systematic biases/errors can exist in the simulations and become difficult to correct. Those errors can be caused by the errors in the initial and boundary conditions, model physics and parametrizations, or inadequate equations or poor numerical methods. When the regional model is coupled with a GCM, it is required that both models should be accurate so as to produce meaningful results. In addition to the Purdue Regional Climate Model, we have presented the results obtained from the nonhydrostatic models, the one-dimensional cloud model, the turbulence-pollution model, the characteristic system of the shallow water equations, etc. Although the numerical model is the most important tool for studying weather and climate, more research should be done on data assimilation, the physics, the numerical method and the mathematic formulation in order to improve the accuracy of the models and have a better understanding of the weather and climate.

1. Introduction

The motion of the atmosphere and ocean can be represented by Navier–Stokes equations, which should be solved numerically. However, the evolution of a weather/climate system consists of motions on many different scales. At the beginning, some of the small disturbances may be described by the linearized equations. When disturbances grow, nonlinear equations become necessary. It is also noted that eigen values/vectors can be easily obtained and interpreted in a linearized system. Hence, for the past few decades, we have been working on linear instability and nonlinear numerical models to study meteorological phenomena, ranging from convection, turbulence, air pollution, cumulus clouds, cloud streets, symmetric instabilities, mountain waves, lee vortices, and land–sea breezes, to synoptic scale waves, barotropic instabilities, cyclones, fronts, and regional climate in East Asia and North America. In order to obtain accurate numerical results, we have also been developing aspects of the model such as the new diffusion equation; turbulence parametrization; snow–vegetation–soil and snow–sea ice packages; forward–backward, advection, and semi-Lagrangian schemes; the pressure gradient force; the multigrid method; the transport of dust and trace gases; and the interaction between aerosols and regional climate. The important components of our mesoscale model are shown in Fig. 1.

We developed the Purdue Regional Climate Model (PRCM). However, several mesoscale regional models exist, with varying approaches. They include the fifth-generation Penn State/NCAR Mesoscale model (MM5; Grell *et al.*, 1995) and the Weather Research and Forecast (WRF) model (Skamarock *et al.*, 2005). Table 1 shows the important features that are used in the PRCM, MM5, and WRF.

A few topics will be briefly discussed here. Many of them require further study. The basic structure of the PRCM and applications will be discussed in Sec. 2, the nonhydrostatic models in Sec. 3, other topics in Sec. 4, and a summary is provided at the end.

2. Purdue Regional Climate Model

2.1. *Basic equations*

The PRCM is a hydrostatic primitive equation model that utilizes the terrain-following coordinate (σ_p) in the vertical direction. It has

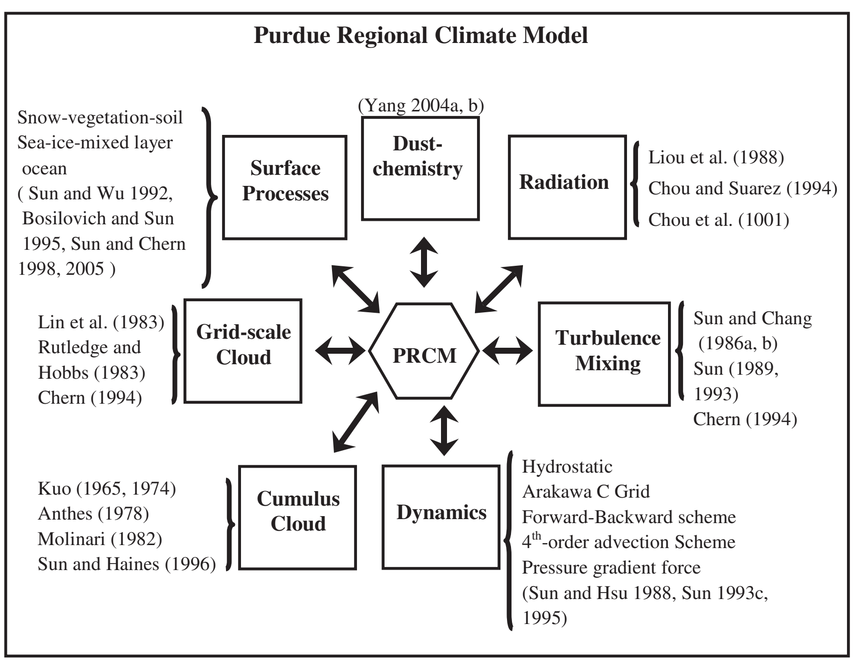

Figure 1. The schematic diagram of Purdue Regional Climate Model.

Table 1. The characteristics of PRCM, WRF, and MM5. WRF has three different dynamical cores. The one that mentioned here is Advanced Research WRF (ARW).

	PRCM	WRF (ARW)	MM5
Hydrostatic/Non-hydrostatic	Hydrostatic	Non-hydrostatic	Non-hydrostatic
Vertical Coordinate	σ_p	σ_p	σ_p
Equations	Advection form	Flux form	Advection form
Time differencing scheme	Forward-backward	Runge-Kutta 3rd order	Leap-frog
Space differencing scheme	4th order or Semi-Lagrangian advection	2nd to 6th order	2nd order
Time step	Timesplitting	Time splitting	Time splitting
Pressure gradient force	Local reference	Universal reference	Universal reference
Thermal variable	Ice equivalent temperature θ_{ei}	Potential temperature	Temperature
Turbulence parameterization	Based on θ_{ei} and total water substances	Based on temperature	Based on temperature

the prognostic equations for momentum; ice-equivalent potential temperature θ_{ei}; turbulent kinetic energy (TKE); surface pressure; all phases of water, including ice, liquid, snow, rain, graupel, and vapor (Lin *et al.*, 1983; Chern, 1994; Haines *et al.*, 1997; Chen and Sun, 2002); and multilayers of soil temperature and wetness, etc. (Sun and Wu, 1992; Bosilovich and Sun, 1995; Chern and Sun, 1998; Sun and Sun, 2004; Sun and Chern, 2005). Because θ_{ei} and total water substance, which are conserved without precipitation, are used as the prognostic variables, the model is able to include a comprehensive turbulence scheme, as discussed by Sun and Chang (1986a,b), Sun (1986, 1988, 1989), Sun (1993a,b), and Chern (1994). The PRCM also includes radiation parametrizations (Liou *et al.*, 1988, Chou and Suarez, 1994; Chou *et al.*, 2001) and cumulus parametrizations (Kuo, 1965, 1974; Anthes, 1977; Molinari 1982). The forward–backward scheme is applied in the Arakawa C grid to permit better computational accuracy and efficiency (Sun, 1980, 1984a). The fourth-order advection scheme (Sun, 1993c) is used to calculate the advection terms. A local reference is applied to calculate the pressure gradient force, which significantly reduces the error of the pressure gradient terms in the σ_p coordinate over steep topography (Sun, 1995a). Recently, the transport of dusts and an atmospheric chemistry module have been added by Yang (2004a,b). We are incorporating the mass-conserved, positive-definite semi-Lagrangian scheme (Sun *et al.*, 1996; Sun and Yeh, 1997; Sun and Sun, 2004; Sun, 2007) and the sea-ice-mixed layer ocean model (Sun and Chern, 1998) into the PRCM, as shown in Fig. 1.

2.2. *Weather simulations*

The PRCM has been applied by Sun and Hsu (1988) to simulate cold air outbreaks over the East China Sea. They showed that the cloud, which has quite different properties than the cold air beneath the cloud base, was formed due to the warm and humid air being lifted by the cold air. This is in good agreement with observations. Hsu and Sun (1991) used the PRCM to simulate one of these cold air outbreak events, reproducing the three-dimensional mesoscale cellular convection, which has a horizontal wavelength of 20–30 km. The model has also been used to study air mass modification over Lake Michigan (Sun and Yildirim, 1989), baroclinic instability and frontogenesis (Sun, 1990a,b), as well as cyclogenesis and the life cycle of cyclones (Yildirim, 1994).

Sun and Wu (1992), applying the PRCM, were the first to successfully simulate the formation and diurnal oscillation of a dryline. Their results show that under a favorable combination of a strong soil moisture gradient, a terrain slope, and a vertical wind shear in Oklahoma and Texas in the late spring and early summer, the dryline can form within 12 hours in the absence of an initial atmospheric moisture gradient. Their results also show that the dryline moves eastward during the daytime, due to a strong mixing of the air near the dryline with the warm and dry westerly wind aloft (which descends from the Rocky Mountains) on the west side, quickly diluting the low level moist air coming from the southeast. At night, the cool, moist air on the east side continues moving into the deep, (still) hot, dry air on the west side, but is no longer vertically mixed and dissipated because the convection ceases to develop due to longwave radiative cooling at the surface. Hence, the dryline moves westward at night, as shown in Fig. 2. Their simulations (Fig. 3) also reproduce a deeper intrusion of the moisture field far above the inversion of the potential temperature field, as observed [Fig. 9 of Schaefer (1974)]. A low-level jet, low-level convergence, and strong upward motion form along the dryline, which are consistent with the inland-sea breeze theory proposed by Sun and Ogura (1979; schematic diagram in Fig. 12 of their paper). These simulations provide an explanation for the frequent occurrence of a dryline in the Great Plains in the late spring and early summer, which becomes a favorable zone for storm development.

Chern (1994) has successfully simulated the two surface low pressures observed with severe winter storms (Fig. 4) in the US, which shut down the highways in the High Plains for a week but, at that time, were poorly predicted by the NWS model. With the PRCM, Haines *et al.* (1997) successfully simulated the ice and super-cooled liquid water observed by aircraft, the lee vortex observed by radar, and surface precipitation of the Denver basin's Valentine's Day storm (VDS) on 13 February 1990.

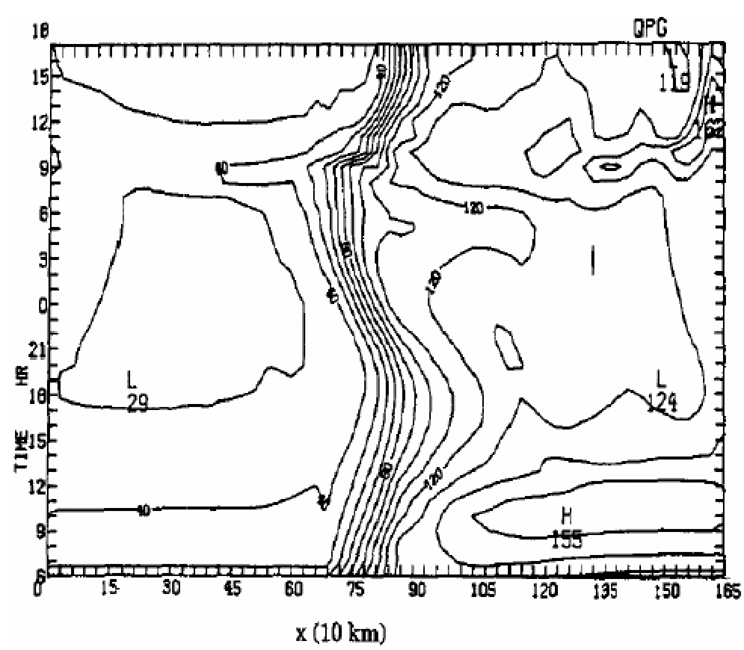

Figure 2. Time-space variation of humidity q_v at $z \approx 10$ m, contour interval of 1 g kg^{-1} labels scaled by 10, dryline moves eastward during daytime but retreats at night (Sun and Wu, 1992).

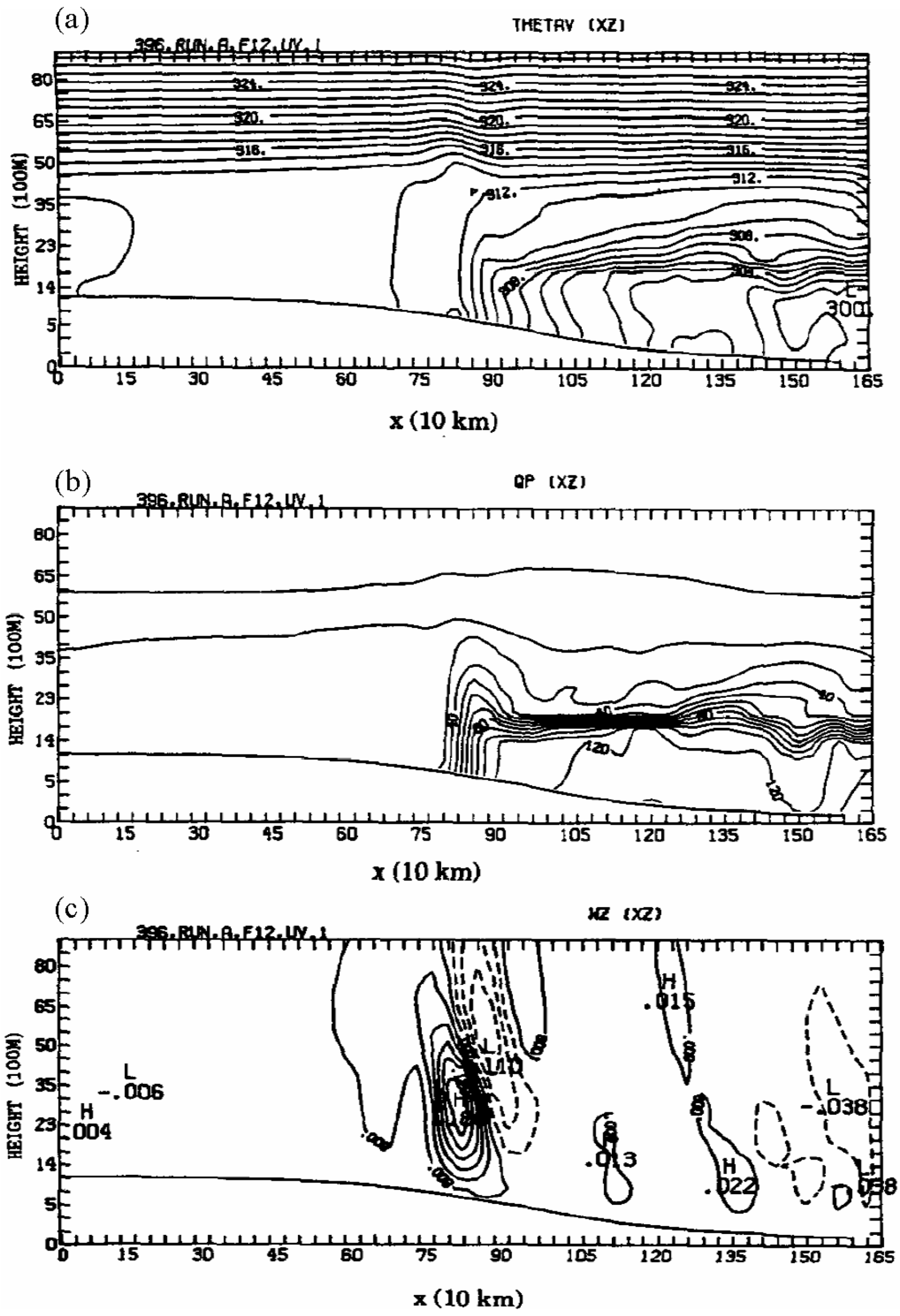

Figure 3. Cross section of the simulated (a) θ_v, (b) total water content q_w, (c) vertical velocity w. The intrusion of the moisture is much deeper than the potential temperature field along the dryline (Sun and Wu, 1992).

(a)

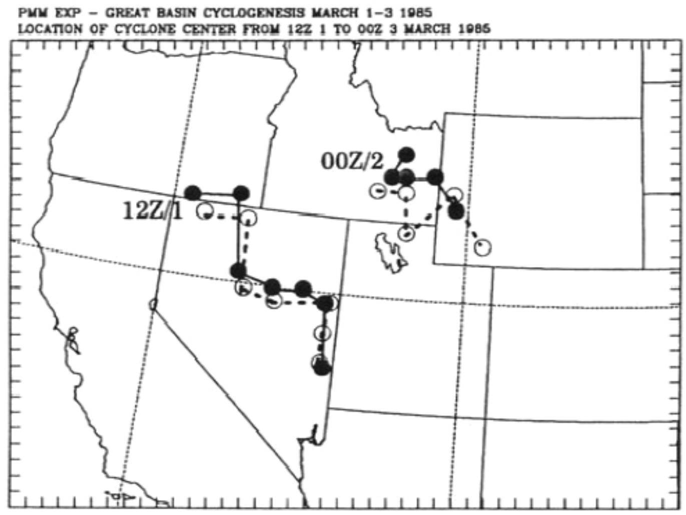

(b)

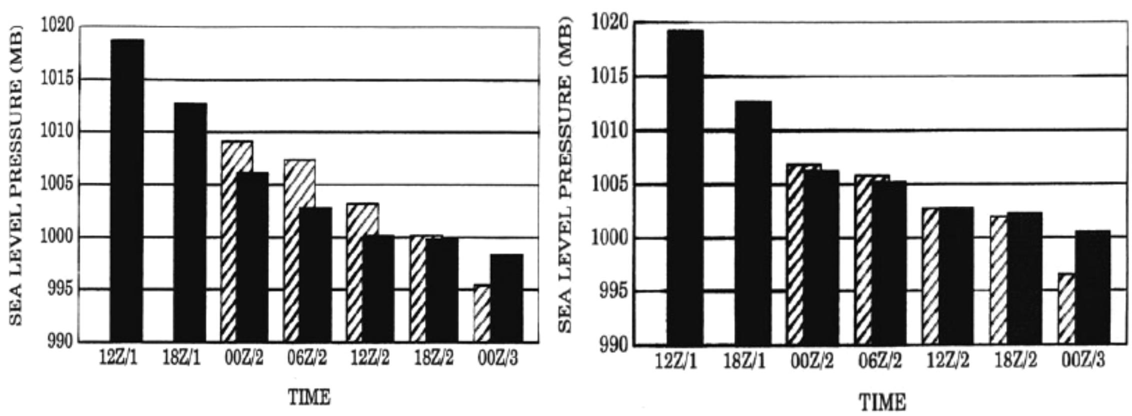

Figure 4. (a) Locations of the cyclones at 6-hr interval. Solid circles represent observation from ECMWF/TOGA analysis. Open from PRCM. The cyclones over Nevada (eastern Idaho) first appeared at 1200 UTC1 (0000 UTC 2) March 1985. (b) Observed (left) and simulated (right) surface pressure at low pressure centers in Nevada (filled bar) and Idaho (hatched bar) (Chern, 1994).

The results show that the PRCM is capable of reproducing the observed mesoscale/synoptic systems, clouds, and precipitation.

2.3. *Applications to Taiwan and East Asia*

Sun *et al.* (1991) applied the PRCM with a free-slip surface to generate a lee vortex and an area of strong wind in northwestern Taiwan under an easterly flow, and a lee vortex to the southeast of the island under a southwesterly flow. The budget of the vertical vorticity component showed that not only the tilting term, as proposed by Smolarkiewicz and Rotunno (1989), but also the stretching and friction terms are important to the formation of lee vortices. With detailed physics and surface parametrizations,

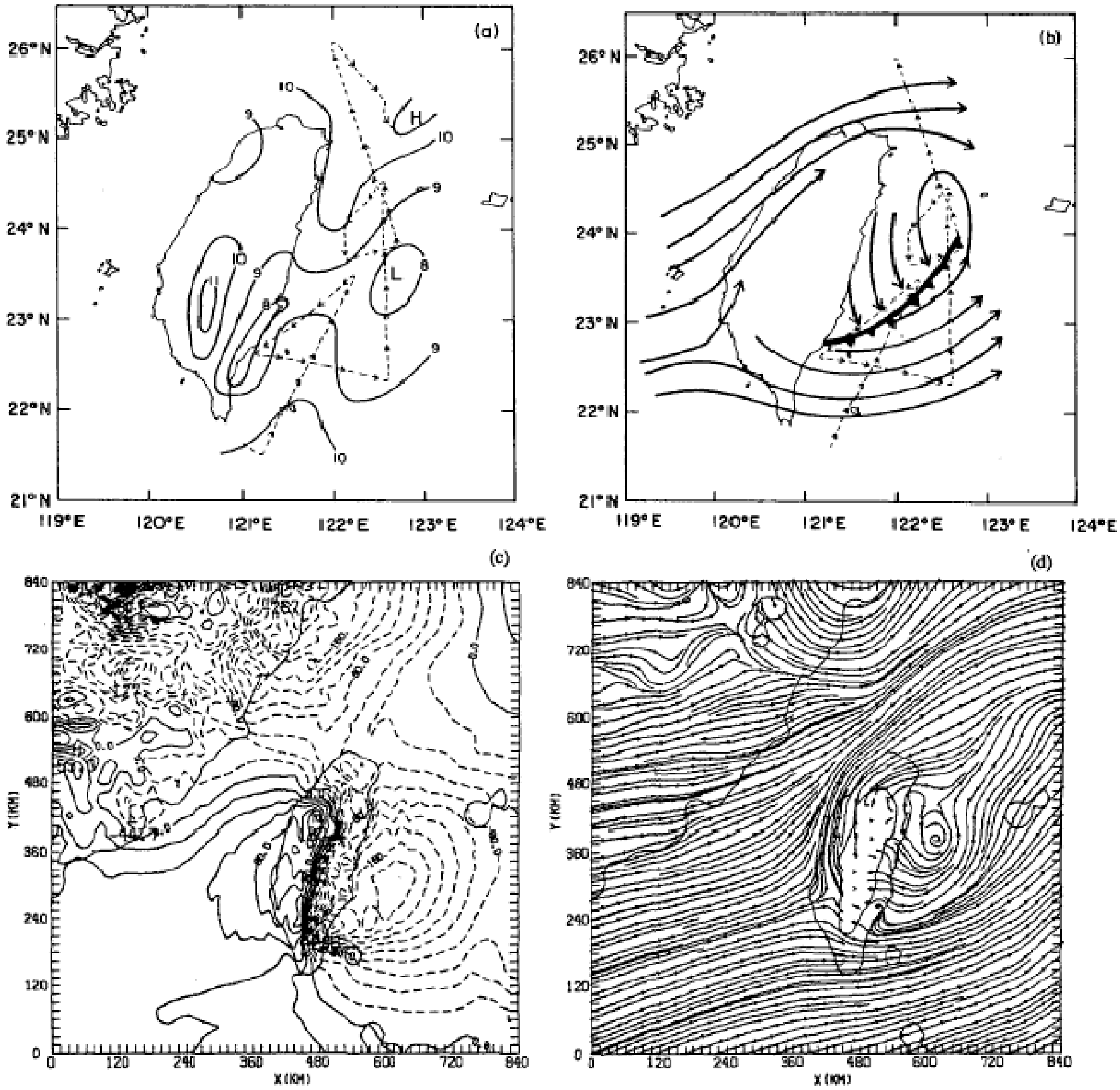

Figure 5. (a) Observed sea surface pressure, (b) observed streamline at 900 mb by airplane (from Kuo and Chen, 1990), (c) simulated sea surface pressure, and (d) simulated streamline at $z = 1$ km at 0200 LST 17 May 1987 (Sun and Chern, 1993).

Sun and Chern (1993) reproduced the observed mesolow, lee vortices, and downslope wind on the lee of the Central Mountain Range (CMR) during TAMEX (Taiwan Area Mesoscale Experiment) IOP(intensive observation period)-2. The lee vortex and the mesolow moved northeastward with time, and were located to the east of Taiwan at 0200LST, 17 May 1987, as shown in Fig. 5. It is also noted that the air moving over the CMR became drier and warmer than the surrounding environment and formed the mesolow to the south of the lee vortex. Hence, no meso-β scale front, which was suggested by Kuo and Chen (1990), developed around the vortex, as shown by smooth streamlines in Fig. 5(d). The model also captured the diurnal oscillation of the land–sea breeze and the formation of the clouds on both sides of the CMR, as observed during fair weather. Furthermore, the existence of mountain waves explains the observed light precipitation on the windward side with a clear sky near the peak of the CMR. Hence, the numerical model can provide plausible physical explanations of phenomena which have otherwise been misinterpreted according to incomplete observational data, such as the mesofront associated with a mesovortex and the distribution of rainfall in Taiwan in that particular situation.

Sun and Chern (1994) further investigated the formation of lee vortices and vortex shedding for low Froude number flow (the Froude number is defined as $\mathrm{Fr} = U/NH$, where U is the mean flow in the upstream, N is the buoyancy frequency, and H is the height of the mountain in a rotational fluid. A pair of symmetric vortices forms on the lee side of the mountain in an irrotational, symmetric flow; but vortex shedding develops in a rotating system, because of the buildup of high pressure from the adiabatic cooling of the ascending motion on the windward side of the mountain, which enhances the anticyclonic circulation and produces a stronger wind on the left side (facing downstream) of the mountain. The anticyclonic flow associated with the relative high on the windward side of the mountain was also observed by Sun and Chern (1993, 2006). Vortex shedding can also be developed by any asymmetry in the wind field, mountain shape, surface stress, etc.

The PRCM also faithfully reproduced the observed severe front during TAMEX IOP-2 (Sun *et al.*, 1995). The well-developed front extended from Japan and the Japan Sea through Taiwan into the South China Sea and Vietnam. The segment of the front between Taiwan and Japan is characteristic of midlatitude fronts, but it is a typical Mei-yu front in the lower latitudes, as reported by Hsu and Sun (1994) and many others: the southern segment has a large moisture gradient but a weak temperature gradient with an accompanying low-level jet on the moist side, which transports moisture from the warm ocean into the system.

In addition to the formation of a lee vortex, the front can be deformed by the CMR, as shown in many satellite images (Chen *et al.*, 2002) and surface maps (Chen and Hui, 1990). Figure 6(a) shows a simulated deformation of the cold front after a 30-hour integration (Sun and Chern, 2006), and Fig. 6(b) is the ECWMF

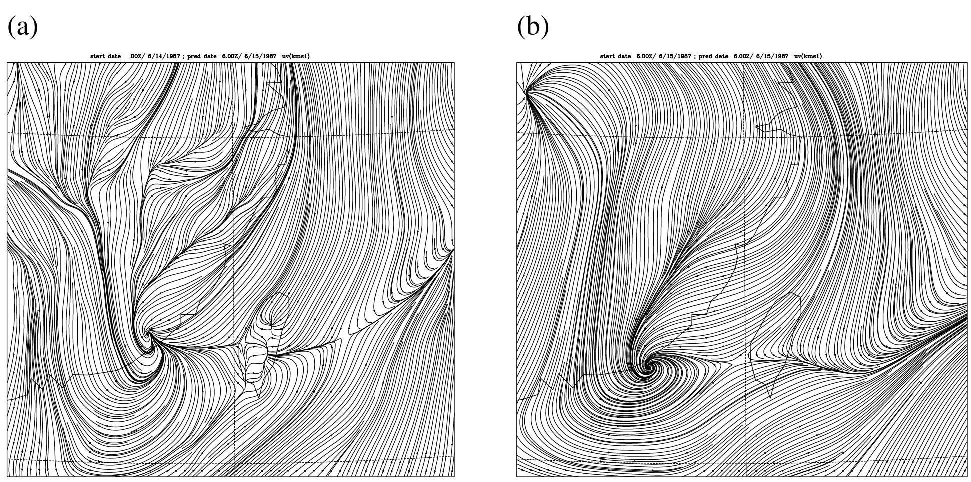

Figure 6. (a) Simulated streamline from the PRCM (after 30 h integration) at 0600 UTC15 June 1987 at $z \approx 25$m; (b) streamline from ECMWF reanalysis (from Sun and Chern, 2006).

reanalysis. The large-scale patterns are quite comparable, except that the deformation of the front by the CMR is missing in Fig. 6(b) due to a lack of observations in the Pacific and/or the coarse resolution used in the ECWMF. The momentum budget shows that the friction, ageostrophic forcing, and nonlinear advection terms are important for the propagation of the front, which has been frequently misinterpreted according to the theory of density current in the irrotational fluid (Chen and Hui, 1990) or trapped Kelvin waves. For more discussion, see Sun and Chern (2006).

2.4. *Regional climate studies*

The results discussed in the previous sections show that the PRCM is a useful tool for forecasting and studying short-term mesoscale and synoptic disturbances. The model has also been applied to study the monthly and seasonal variations of regional climate and the hydrological cycle. Bosilovich and Sun (1999a,b) applied the PRCM to study the 1993 summer flood in the Mississippi Valley. The model reproduced the observed precipitation associated with the transient synoptic waves in June and the Mesoscale Convective System (MCS) in July (Fig. 7) due to a change in atmospheric stability. Sensitivity tests showed that without the local surface source of water vapor, the flooded region's atmospheric hydrological budget reduced to an approximate balance between precipitation and moisture flux convergence. Comparisons with the control simulation hydrology estimated that 12% and 20% of precipitation had a local source for June and July 1993, respectively (Bosilovich and Sun, 1999b).

Many scientists have applied numerical models to study the cause(s) of this drought. However, discrepancies exist among the different hypotheses. For example, Oglesby and Erikson (1989) and Oglesby (1991) demonstrated the persistence of an imposed soil moisture anomaly in the US using National Center for Atmospheric Research Community Climate Model 1 (NCAR-CCM1). However, also using NCAR-CCM1, Sun *et al.* (1997) carried out four experiments, including using the climatological SSTs (control case), 1988 SSTs, dry soil moisture anomaly (25% of soil moisture in May in the normal year between 35 and 50°N in the US), and 1988 SSTs and dry soil moisture anomaly, to study the effect of SST and soil moisture. For each experiment, three model simulations were performed and were initialized from arbitrary conditions. The results show that the 1988 SST did not cause the simulated weather pattern over the US to be drier than the control case with climatological SST. The ensemble mean with perturbed soil moisture experiment did show less precipitation than the control; however, due to the large variance in the data, the reduction in precipitation was not statistically significant.

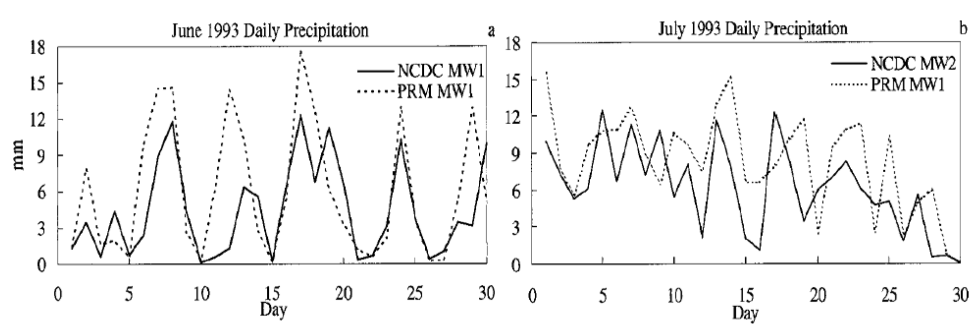

Figure 7. Simulated from PRCM and NCDC observation of daily integrated precipitation over flooding area in the midwestern US for: (a) June associated with synoptic waves and (b) July 1993 associated with mesoscale convective system (Bosilovich and Sun, 1999a).

The experiment with the soil moisture anomaly and 1988 SST obtained the most significant differences, specifically in the reduction of precipitation in the US. This may indicate that the 1988 severe drought may have been caused by a combination of dry soil and a special large scale weather pattern related to the SST, rather than by either the SST or dry soil alone.

Using the observed SST and the ECMWF analysis as initial and lateral boundary conditions, the PRCM (Sun *et al.*, 2004) reproduced a strong warm ridge at 500 hPa in North America over a hot, dry land. The monthly precipitation and soil moisture were far below the normal values in the Midwest and the Gulf states, but above normal in the Rocky Mountains, consistent with observations. It is noted that the PRCM reproduces not only the waves passing through the lateral boundaries, but also the development and decay of the disturbances inside the domain, which are not shown here. A sensitivity test also shows that monthly precipitation could significantly increase using the saturated soil moisture as the initial condition. However, the soil would dry up eventually, because the wet soil does not provide a positive feedback with the low-level jet. Hence, the large-scale weather pattern in the early summer of 1988 might have triggered the dry episode by forming a ridge in North America. This ridge gradually cut down precipitation in the Gulf states and Midwestern region. The soil became dry and hot, which further intensified the blocking of the warm ridge in the US. Hence, dry soil had a positive feedback on the severe drought in the summer of 1988. But the dry soil alone was not the cause of the drought, for in spite of even less soil moisture in early July, observed precipitation amounts returned to normal after mid-July 1988.

Min (2005) recently applied the PRCM with the new snow-land-surface module developed by Sun and Chern (2005) to study the 1997 spring flooding in Minnesota and the Dakotas due to spring snowmelt. With a wet soil, the north-central US experienced horrific conditions over the winter of 1996–97. An enormous snow pack was built up by blizzard after blizzard from the second half of November through January; many areas had more than 250 cm of snowfall. These amounts were as much as 2–3 times the normal annual amount. Although February and March were quite dry, frigid conditions throughout much of the winter ensured that as much as 25 cm of snow water equivalent remained on the ground when the spring melt period began in March. Early March brought temperatures below normal, delaying the onset of snowmelt. Significant melt of the deep snow started with particularly warm conditions at the end of March and in early April. At this time, many rivers in South Dakota, southern Minnesota, and southern North Dakota were rising, in some cases well above the flood stage. With a comprehensive snow–soil physics included in the PRCM, the simulated results of snow depth and precipitation rate can be dramatically improved (not shown in the figures). Our study revealed the importance of the detailed physics/parameters in a model, which can influence results in faraway regions. In addition, we also showed that the land properties can affect the flow pattern in the upper level as high as 200 hPa.

The PRCM has also been applied to study the East Asia Monsoon and short-term regional climate, by Sun and Chern (1999), Sun (2002), Hsu *et al.* (2003), Yu *et al.* (2004a,b), Hsu *et al.* (2004), etc. Figure 8 shows that the jet at 850 mb migrated northward over the summer of 1998 (Sun and Chern, 1999). Heavy precipitation occurred in Central China in midsummer, moving to Korea and northern and northeastern China in August. The front and the low-level jet dissipated after mid-August, as observed.

In simulations of the heavy flooding over Korea and China between 30 July and 18 August 1998, the model results show that the heavy rainfall along the Baiu/Mei-yu front was due to a combination of: (1) an anomalous

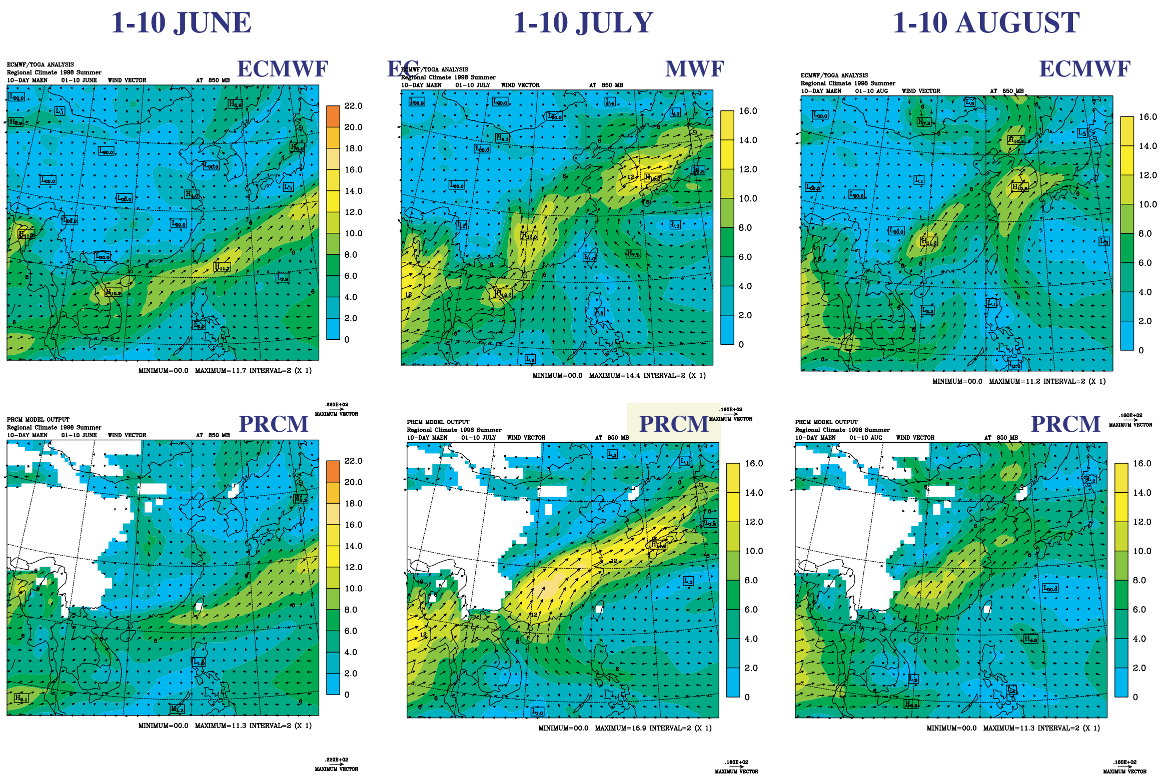

Figure 8. Ten day mean wind vector and isotachs (ms^{-1}) at 850 mb for the first 10 days of June, July, and August of 1998 (Sun and Chern, 1999).

850 hPa subtropical high, (2) a stronger baroclinicity around 40°N over eastern Asia and a low pressure located to the north of the front, and (3) excessive evaporation from the abnormally wet, warm land (Sun, 2002). The precipitation ended on 18 August, when the subtropical high retreated and the low pressure in Manchuria moved away from the Asian continent. The model reproduced well the observed baroclinic waves to the north, the subtropical high and low-level jet to the south, and the front with heavy precipitation extending from southern China and the Korean peninsula to Japan. High correlations (Table 2) were also found for most variables between the model simulation and the ECMWF reanalysis for the 20-day means. However, it is also noted that the simulated low pressure in Manchuria, which was to the north of the Mei-yu front, propagated more slowly than observed, which may be responsible for the deepening of this low as well as for excessive heavy precipitation in the area (Fig. 9). It is also noted that the model generated a wet bias of precipitation in mountainous areas and a too strong subtropical high in the Pacific.

The PRCM also reproduced well the spatial distribution of mean surface temperature and mean sea level pressure during ten summers over East Asia as well as the temporal variation of mean vorticity over the South China Sea (Fig. 10; Yu *et al.*, 2004a,b; Hsu *et al.*, 2004).

2.5. *Simulations of dust and ozone*

Regional models coupling atmospheric chemistry have been applied with the PRCM to predict the transport and dispersion of trace gases and aerosols. Yang (2004a) has coupled the

Table 2. 20-day mean statistics of PRCM compared with ECMWF (Sun 2002).

FIELD	LEVEL	BIAS	RMS	COR
Mean Sea Level Pressure	SFC	−4.80E+01	1.57E+02	0.95
AirQv (kg/kg)		2.45E−03	2.81E−03	0.96
Temperature (K)		7.33E−01	1.75E−00	0.97
Wind vector		7.81E−01	1.26E−00	0.84
Height (m)	200 hPa	3.70E+01	4.51E+01	0.99
	500 hPa	1.25E+01	1.77E+01	0.98
	850 hPa	2.54E−01	1.03E+01	0.97
Temperature (K)	200 hPa	7.44E−01	1.17E−00	0.9
	500 hPa	6.30E−01	8.55E−01	0.98
	850 hPa	1.32E−01	1.22E−00	0.94
Qv (kg/kg)	500 hPa	−1.34E−04	6.59E−04	0.83
	700 hPa	3.01E−04	1.22E−03	0.82
	850 hPa	1.13E−03	1.61E−03	0.92
Wind vector	200 hPa	−1.60E−00	3.98E−00	0.91
	500 hPa	−7.21E−01	2.14E−00	0.8
	850 hPa	1.28E−00	2.16E−00	0.83

(a) (b)

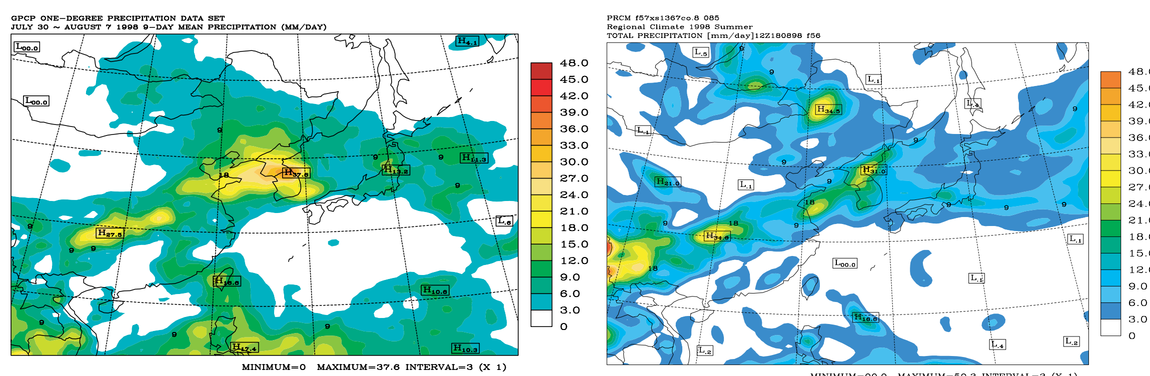

Figure 9. (a) GPCP day mean precipitation; and (b) simulated day mean precipitation during July 30–August 18, flooding spread in Manchuria, Korea, and Yangtze River Valley. The model missed the tropical depression from southern boundary due to the coarse resolution (Sun, 2002).

PRCM and the dust/chemistry module as illustrated in Fig. 11 to simulate the distribution of aerosols and the interactions between aerosols and regional climate during April 1998.

The dust module consists of: (a) a dust source function derived by Ginoux *et al.* (2001) based on a 1°-by-1° terrain and vegetation data set derived from Advanced Very High Resolution Radiometer (AVHRR) data (DeFries and Townshend, 1994); (b) particle sizes, which are a function of the source region's soil properties (Tegen and Fung, 1994); seven-size bins (0.1–0.18 μm, 0.18–0.3 μm, 0.3–0.6 μm, 0.6–1 μm, 1–1.8 μm, 1.8–3 μm, and 3–6 μm, with corresponding effective radii of 0.15, 0.25, 0.4, 0.8, 1.5, 2.5, and 4 μm) are applied for dust sizes (Yang, 2004a); (c) the threshold friction velocity, defined as the horizontal wind velocity required to lift dust particles from the surface, is a function of particle diameter (Marticorena and

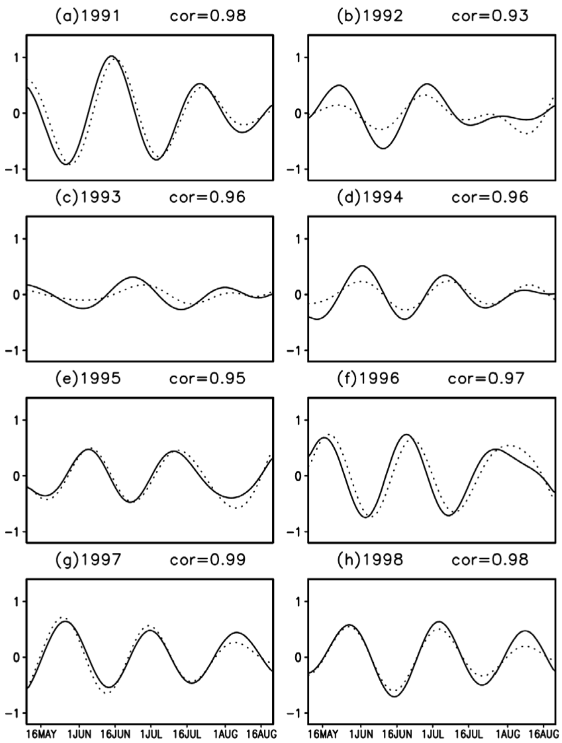

Figure 10. The mean vorticity over South China Sea (15–20°N; 110–120°E) during May–August from 1991–1998, solid lines are calculated from ECMWF analysis and dashed lines are PRCM results (Yu *et al.*, 2004a,b). Correlation coefficients between ECMWF analysis and PRCM results for individual years are also shown in each panel.

Bergametti, 1995) and soil wetness; (d) dust emission, which depends on source function, surface wind speed, threshold velocity, and the fraction of each size class; and (e) transport and removal processes — dust aerosols in the PRCM dust are transported by advection, dispersion, and subgrid cumulus convection, and are removed by wet and dry depositions. The dry deposition of dust aerosols is assessed through the gravitational settling for each model vertical layer and surface deposition velocity. The removal of dust aerosols by wet deposition is calculated using the model precipitation rate at all model levels, for both stratified and convective clouds. PRCM dust is capable of reproducing observed weather and satellite images of dust during the 17-day continuous integration of April 1998 (not shown in the figures).

Yang (2004b) also included the chemistry mechanism of SAPRC97 (Statewide Air Pollution Research Center) (Carter *et al.*, 1995, 1997), which is a detailed mechanism for gas-phase atmospheric reactions of volatile organic compounds (VOCs) and oxides of nitrogen (NO_x) in urban and regional atmospheres. Coupling SAPRC97 and PRCM dust, Yang (2004b) showed that the model can reproduce the observed ozone concentration in the sky and at the surface in the US after a spin-up period of two days.

Wu *et al.* (2003) and Hsu (2001) applied the PRCM to study the transport of pollutants from a point source at the northern tip of Taiwan during four seasons in 1999. Figures 12(a) and 12(b) show the observed and simulated wind (after 48-hour integration) at 12Z on 31 October 1999; while the schematic diagram of pollutant transport and the vertically integrated concentration from the PRCM for the same time are shown in Figs. 12(c) and 12(d), respectively. They indicate that the plume moves around the western coast, the eastern coast, or even the entire island, depending on the detailed wind speed and direction under northerly wind.

3. Nonhydrostatic Models

3.1. *Basic equations*

In recent years, we have developed two nonhydrostatic models suited for studying a wide range of spatial scales of atmospheric systems. Both models are based on a fully compressible fluid in a terrain-following vertical coordinate. The National Taiwan University (NTU)/Purdue Nonhydrostatic Model (Hsu and Sun, 2001) is an explicit model in terms of its time integration scheme, while the other model (Chen and Sun, 2001), using a semi-implicit scheme, is an implicit model.

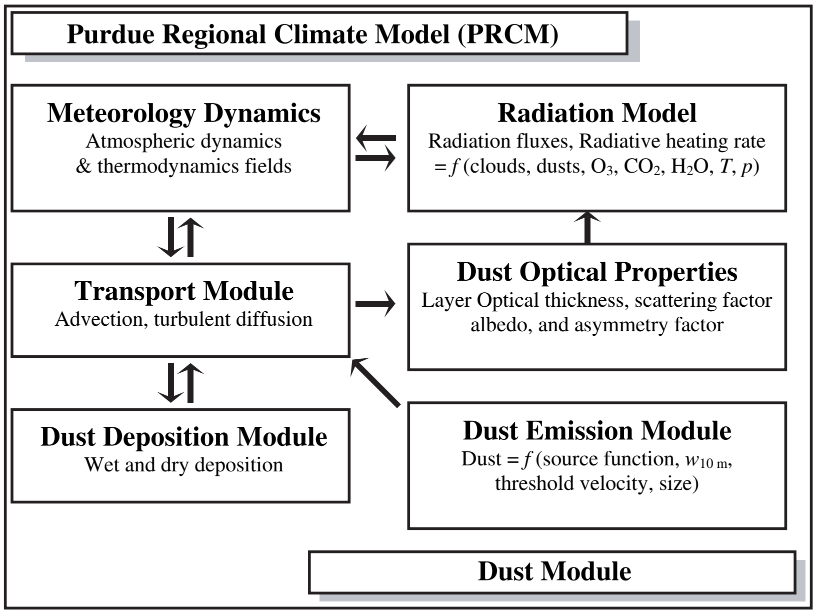

Figure 11. The schematic illustration of the components in the integrated PRCM-dust Model (Yang, 2004a).

The NTU/Purdue Nonhydrostatic Model uses a double forward–backward time integration procedure for treating both sound waves and internal gravity waves. The algorithm is stable, and does not generate computational modes. Although the integration time step is very small due to the CFL criterion imposed by treating high-frequency sound waves explicitly, this shortcoming is mitigated by using a time-splitting scheme and parallel computing. The explicit integration procedure is particularly well suited for parallel computing since a minimal amount of data transfer among CPUs is required with all partial differentiations calculated through local grid points. With the help of the National Center for High-performance Computing (NCHC) in Taiwan, the of has been written in Fortran 77 and Message Passing Interface (MPI) codes so that it can work on both supercomputers and PC clusters. The efficiency of the parallel processing depends on the number of grid points used in a simulation and the characteristics of the particular atmospheric circulation simulated. In one of the simulations with no clouds, our model achieved over 95% efficiency for a 128-processor job (Hsu *et al.*, 2000). The high efficiency allows us to apply the model in studying resource-demanding problems, such as turbulence and local circulations.

In addition to its basic dynamic framework, the NTU/Purdue Nonhydrostatic Model takes into account many physical processes, such as land/ocean processes, cloud microphysics and atmospheric turbulence. The prognostic thermodynamic variables are the same as in the PRCM, with the addition of density in the continuity equation. The NTU/Purdue Nonhydrostatic Model is, thus, quite compatible with the PRCM. It will be possible in the future, with the improving computer technology, to nest the two models together for studying problems involving multiple-scale interactions.

Chen and Sun (2001) (CS) applied a multigrid solver in the Purdue Nonhydrostatic Model, which is a semi-implicit time integration scheme and can have a much larger time interval than that used in the NTU/Purdue

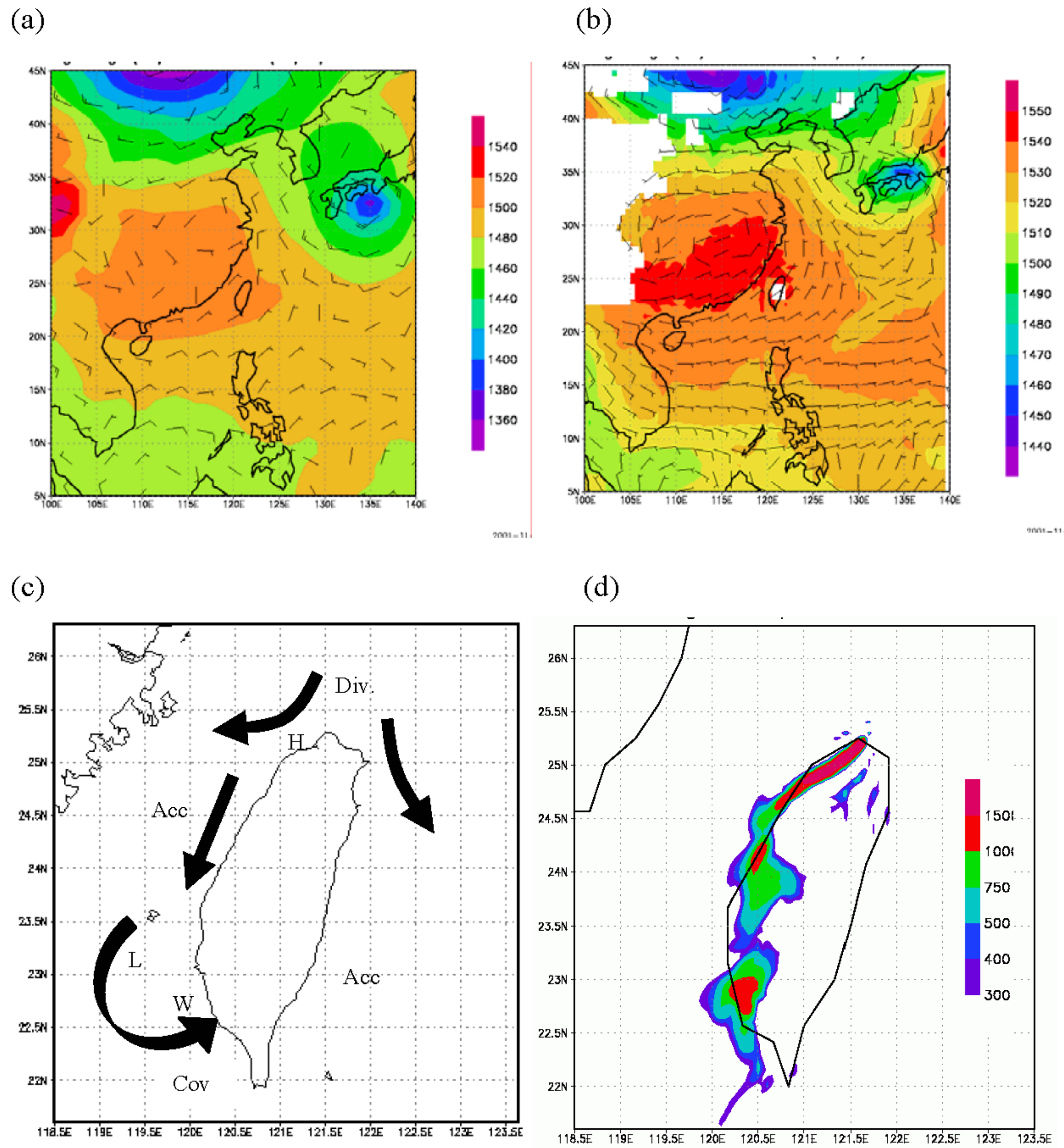

Figure 12. (a) ECWMF-reanalysis wind at 850 mb at 1200 UTC 31 Oct 1999, (b) same as (a) except for PRCM simulation (after 48 h integration), (c) schematic diagram of pollutant transport under northerly, and (d) vertical integrated concentration at 1200 UTC 31 Oct 1999 (after 48-h integration) (Wu *et al.*, 2003, Hsu, 2001) (Div: divergence, Acc: accelerateion, Con: convergence, W: westerly wind, H: high pressure, and L: low pressure).

Nonhydrostatic Model. In addition, a flexible hybrid coordinate in vertical was designed and used in that model. The two nonhydrostatic models produced consistent results for mountain waves, thermal convection, etc. The complicated multigrid approach has shown great potential for future development of nonhydrostatic models.

3.2. *Flow over mountains*

3.2.1. *Linear mountain waves*

Both (NTU/Purdue and CS) nonhydrostatic models have been validated with steady-state analytical solutions in several linear mountain wave situations, such as the two-dimensional, nonhydrostatic solution in Queney (1948); the two-layer, trapped-wave situation (Scorer, 1949); and the three-dimensional, nonhydrostatic situation (Smith, 1980). The model results are very close to the analytical solution in all cases. Figure 13 shows the horizontal distribution of the potential temperature anomaly, which is inversely proportional to the vertical displacement of airflow passing over a bell-shaped mountain at a height close the ground surface. The 2-hour simulation result is in good agreement with the analytical solution.

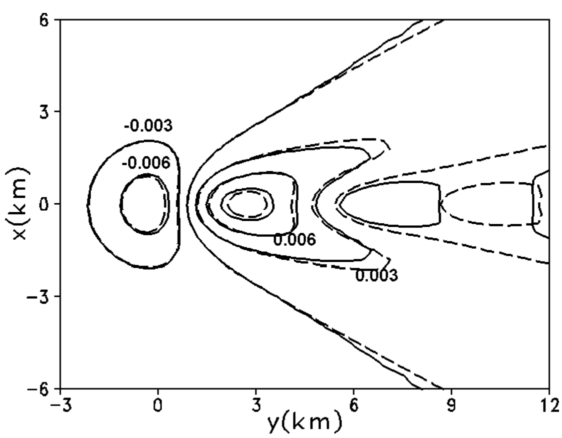

Figure 13. Horizontal distributions of the potential temperature anomaly for airflow passing over a bell-shaped mountain at the non-dimensional height of $Nz/U = \pi/4$. Solid contour lines correspond to the model result after 2 h. The grid interval is 300 m in all three directions. The dashed contour lines represent the analytical, steady-state solution in Smith (1980). The center of the bell-shaped mountain is located at the (0, 0) coordinate. The linear mountain waves is nonhydrostatic with $Na/U = 1$. The vertical static stability, mean wind speed and the half-width length of the mountain are $N = 0.01\,\mathrm{s}^{-1}$, $U = 10\,\mathrm{m\ s}^{-1}$ (from left to right in the figure), and $a = 1$ km, respectively. The contour interval is 0.003 K.

Hsu and Sun (2001) also found an error in Queney's classic 1948 paper. The surface pressure distribution in the two-dimensional, nonhydrostatic, linear mountain wave solution is off by about 100%, and the vertical displacement plotted in the original paper is not accurate either. The erroneous diagram has been cited repeatedly in many books (Gill, 1982; Smith, 1979) and papers over half a century. Our results, which have been confirmed by Chen and Sun (2001), can serve as a basis for future nonhydrostatic model development.

3.2.2. *11 January 1972 Boulder windstorm*

Both nonhydrostatic models have been used to simulate the famous 11 January 1972 Boulder windstorm (Lilly, 1978). The models reproduced the strong downslope wind and hydraulic jump for both free-slip surface and viscous surface simulations. With a free-slip boundary, the simulated hydraulic jump propagates downstream; however, the jump becomes stationary with a more realistic no-slip boundary condition (Fig. 14). The maximum wind also differs, depending on the lower boundary. For a viscous surface, it is around 45–50 m s^{-1}, compared with 70 m s^{-1} or more for a free-slip surface (Sun and Hsu, 2005).

3.2.3. *White Sands simulation*

The NTU/Purdue model was applied to several well-observed real terrain cases for local circulations over the Organ Mountains in White Sands, New Mexico, USA, using 1 km grid resolution. The model successfully simulated strong winds over the valley, lee vortices, and downdrafts on the lee side for a weak prevailing wind situation (not shown in the figure). On the other hand, waves of strong–weak surface winds were simulated on the lee under a strong prevailing wind. The simulated wind patterns have been confirmed by upper air soundings and surface observations (Haines *et al.*, 2003). Oh (2003) also

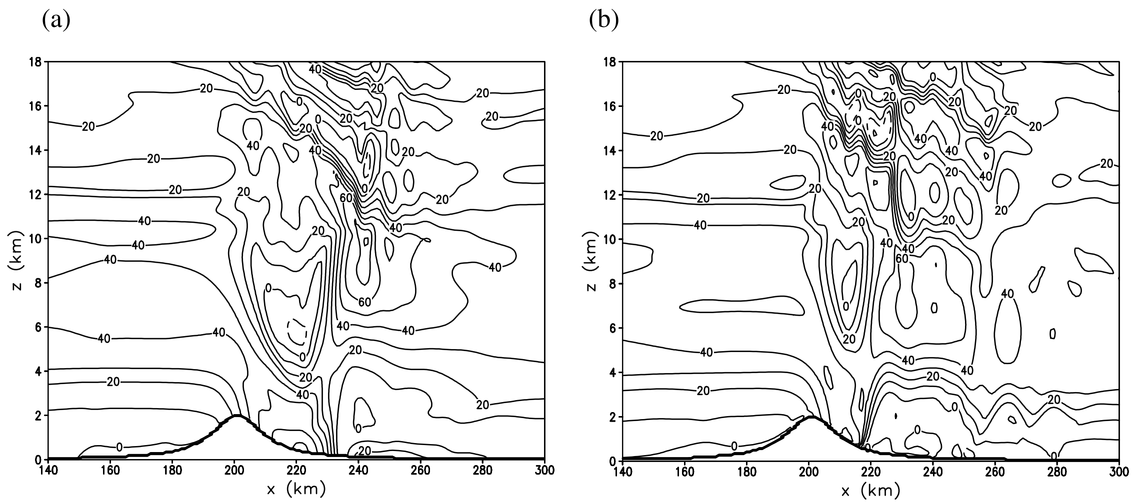

Figure 14. Simulated u-component wind for a 2-km mountain after 2.5 h of integration: (a) free-slip surface and (b) rigid surface (Hsu and Sun, 2001, and Sun and Hsu, 2005).

applied this model to study the flow over an idealized, bell-shaped mountain under different environments.

3.3. *Large eddy simulation (LES)*

With the use of an open lateral boundary and a very large number of grid points in the NTU/Purdue Nonhydrostatic Model, Hsu *et al.* (2004) were able to simulate the development of stratocumulus in a heterogeneous environment during a cold air outbreak event. A convective boundary layer (CBL) develops as very cold air originating from Siberia and China flows over the Japan Sea, the Yellow Sea, and the East China Sea during winter seasons. The CBL quickly deepens away from the coastline, with increasing fetch length and sea surface temperature. As the depth of the CBL changes, the embedded roll vortices (cloud streets) grow in size. The convection eventually becomes three-dimensional in the downstream region. The simulated convection also shows both 2D rolls and 3D cells in our simulation (Fig. 15). The increase of the CBL's depth and strength may result in changing cloud shapes.

4. Other Topics

4.1. *Turbulence, pollution and PBL*

In a higher-order turbulence parametrization, Sun and Ogura (1980) introduced a turbulence length scale in the stable layer that is related to the atmospheric stratification. They also included the equation for the potential temperature–humidity covariance $(\overline{\theta' q'})$ and were able to simulate the observed $(\overline{\theta' q'})$ and some third-order terms. Sun and Chang (1986a,b) and Sun (1986, 1988, 1989) extended Sun and Ogura's work by including the temperature-concentration covariance and using the observed turbulence length scale in the CBL (Caughey and Palmer, 1979) as a length scale in the model, successfully simulating the transport and dispersion of plumes in a convective boundary layer. Simulated results (Sun, 1988, 1989) were compared with the laboratory study by Deardorff and Willis (1975) for pollution released from point sources at different heights. Both laboratory and model simulations show that the plumes move upward from the point source near the surface, but the plumes from the elevated point sources descend quickly and form a high concentration zone near the

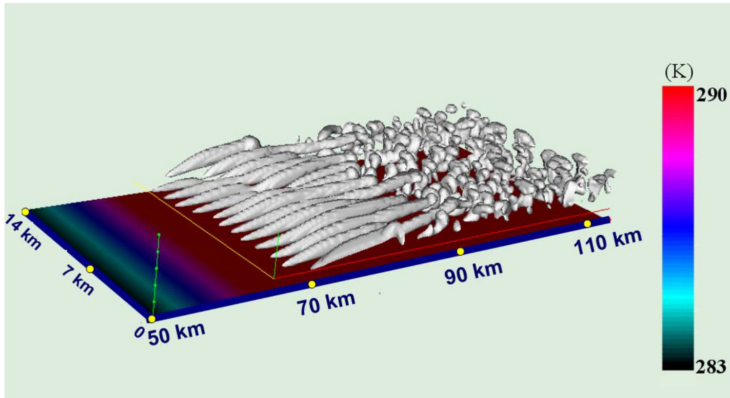

Figure 15. The simulated stratocumulus after 2-h integration during a cold air outbreak over a warm ocean. The background color shows the sea surface temperature distribution (scale indicated to the right of the figure; units in K). The thin red and orange lines identify the lowest cloud level at $z = 300\,\text{m}$. Cold air with temperature of 280 K near surface comes from the left with wind speed of $10\,\text{m s}^{-1}$. Cloud streets broke into three-dimensional cells in the downstream region. The grid intervals in x, y and z directions are 200, 100, and 50 m, respectively (Hsu *et al.*, 2004).

surface before they move upward. The modeled mean plume height and the surface concentration were also comparable with observations (Willis and Deardorff, 1978, 1981). Sensitivity tests show that the temperature-concentration covariance is crucial to turbulence-pollution modeling, which had been ignored before. The simplified version of this turbulence parametrization is also used in the PRCM (Chern, 1994). Currently, MacCall (2006) is working on the third-order turbulence closure to study the turbulence in a stable boundary layer.

4.2. *Snow–vegetation–soil*

A comprehensive snow–vegetation–soil module has been developed for the PRCM (Wu and Sun, 1990a,b; Sun and Wu, 1992; Sun, 1993a,b; Bosilovich and Sun, 1995; Sun and Bosilovich, 1996; Bosilovich and Sun, 1998; Chern and Sun, 1998; Sun and Chern, 2005). It handles diffusion and transport of heat and water substance inside snow, vegetation, and soil as well as the processes of melting and freezing and the fluxes at the interfaces, etc. Figure 16 shows a comparison between the observations and model simulations of the soil temperature during summer. Sun and Chern (2005) simulated the changes of the snow depth and soil temperature in the Sleepers Watershed Experiment during 1969–1974. The simulations are in good agreement with observations.

4.3. *Cloud streets and symmetric instability*

Kuo (1963) applied the linear theory to explain the cloud streets observed in a trough in the easterly wave (Malkus and Riehl, 1964). He successfully simulated the cloud streets forming along the wind shear in a dry, unstable atmosphere with a constant lapse rate, but failed to produce the larger cloud streets forming perpendicular to the wind shear. Using the real atmospheric stratification and including the effect of latent heat release, Sun (1978) demonstrated that observed clouds may be explained by the coexistence of two different types of clouds: the shallow convective-type cloud streets form along the wind shear, and the deep wave-type cloud streets develop perpendicular to the wind shear.

Sun and Orlanski (1981a,b) solved both linearized and nonlinear equations as initial value problems and confirmed that the two-day waves can be easily excited by the diurnal

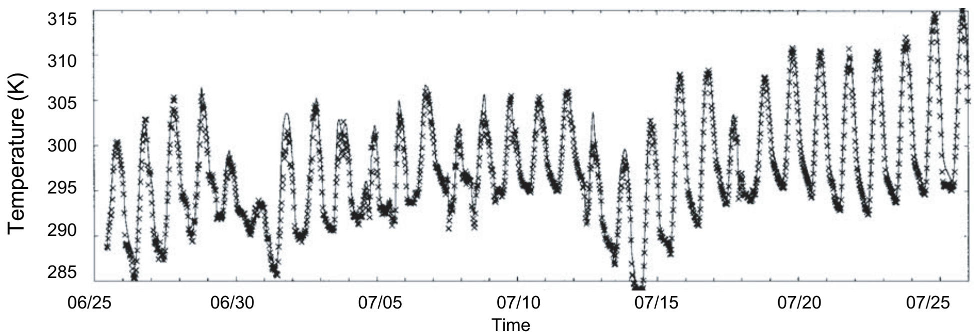

Figure 16. Comparison of model-simulated surface temperature (solid line) and observations (symbol x) during FIFE campaign, 25 June–25 July 1987 (Bosilovich and Sun, 1998).

oscillation of the land–sea contrast at lower latitudes (<15°). On the other hand, one-day and two-day waves may coexist at latitudes of up to 30°. These waves may correspond to the mesoscale cloud bands observed along coastlines with a space interval of a few ten to a few hundred kilometers (Fig. 1 in Sun and Orlanski, 1981a).

Integrating the linearized equations as a wet-symmetric instability problem, Sun (1984b, 1987) showed that the small-sized rainbands can organize into larger ones with strong narrow upward motions interspersed with weak and widespread downward motion, because the ascending air should be warmer than the descending air parcel to maintain the positive circulation. Those rain bands also propagated toward the warm side, which is the source of moisture in a rotating fluid. Sun (1995b) further proved that the y component of the earth rotation ($2\Omega \cos\phi$; where ϕ is the latitude) can significantly impact the growth rate of symmetric instability in the lower latitudes, because the x component wind u can either enhance or decrease the z component acceleration through the $u\ 2\Omega\cos\phi$ term in the momentum equation.

4.4. *Cumulus parametrization scheme (CPS) and cloud models*

Haines and Sun (1994) developed a simple steady 1D cloud model to be used in the cumulus parametrization scheme (Sun and Haines, 1996). This CPS also includes the Weisman and Klemp (1984) storm intensity according to the wind shear and buoyancy environment and allows three sizes, of clouds: small, medium, and large sizes, with different radius and cloud depth. The population of each cloud type is determined by the conservation of mass and moisture flux, and the ability to generate the fastest heating rate from the combined clouds. The CPS has been tested against the SESAME V storm-scale analysis from 2000 UTC to 2300 UTC on 20 May 1979, when the precipitation was almost exclusively convective in nature. They are in good agreement in the apparent heat source (Q1) and the apparent moisture sink (Q2), as shown in Fig. 17 for both strong and weak convections. The CPS was also successful in diagnosing the apparent heat source (Q1) and the apparent moisture sink (Q2) from purely convective sources even later in the SESAME V case, when a significant amount of stable type precipitation developed. The CPS has been incorporated in the PRCM to simulate the squall line observed during SESAME V. The simulated squall line formed about when and where the observed squall line did. Additionally, later deep convection to the south along the dry line was successfully simulated. However, it is very important and challenging to develop a better CPS with more rigorous assumptions and formation.

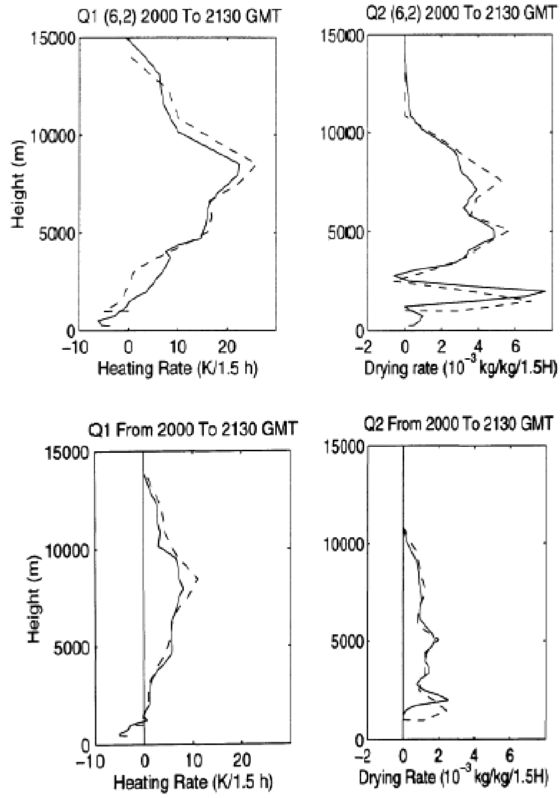

Figure 17. Comparison of observed (solid) and CPS diagnosed (dashed) from 2000–2130 UTC, 20 May 1979 for Q1 and Q2 at two locations during SESAME V experiment (Sun and Haines, 1996).

In order to avoid using a steady state cloud model as in Haines and Sun (1994), Chen and Sun (2002) have developed a time-dependent one-dimensional cloud model, which represents well the average properties of the clouds generated by the WRF model (Fig. 18). Furthermore, Chen and Sun (2004) developed a one-dimensional time-dependent tilting cloud model to represent the effect of wind shear. Hopefully, those cloud models can be incorporated into the CPS in the near future.

4.5. *Barotropic model and shear instability*

Sun and Chang (1992) applied a nonlinear barotropic model to study the barotropic instability (Kuo, 1949) of the modified hyper-tangent shear flows, which may represent the flow along a Mei-yu front or a cyclone family in the middle-to-high latitudes. In a β plane, the waves initially propagate as Rossby waves through the various basic states following linearized equations. Those waves move into the most unstable zone and, thus, grow more rapidly than in the weak shear zone. In the later stage, the nonlinear wave interaction becomes dominant and the transition among the modes becomes very difficult to predict. The simulations confirm that the results are very sensitive to external forcing, the basic wind field, the effect of β, as well as the initial perturbation field. This may suggest that predictability is very limited even in this simple 2D barotropic flow. The evolution of 2D shear flow has also been studied by Oh (2007) using the semi-Lagrangian scheme on the characteristic shallow water equations.

4.6. *Numerical schemes*

The results of a numerical prediction model depend upon the model equations, the physics, the initial and boundary conditions, and the numerical methods. Therefore, we have also been working on numerical schemes in order to provide more accurate results. In addition to diffusion equations (Sun, 1982) and a forward–backward scheme for inertial–internal gravity waves (Sun, 1980, 1984a), Sun developed an advection scheme which is more accurate than the popular Crowley fourth-order advection scheme (Crowley, 1969). Sun *et al.* (1996), Sun and Yeh (1997), and Sun and Sun (2004) also developed a mass-conserved, positive-definite semi-Lagrangian scheme. A forward trajectory and simple mass correction are applied in this scheme. The procedure includes: (a) constructing the Lagrangian network induced by the motion of the fluid from the Eulerian network and finding the intersections of the networks by a general interpolation from the irregularly distributed Lagrangian grid to the regularly distributed Eulerian grid,

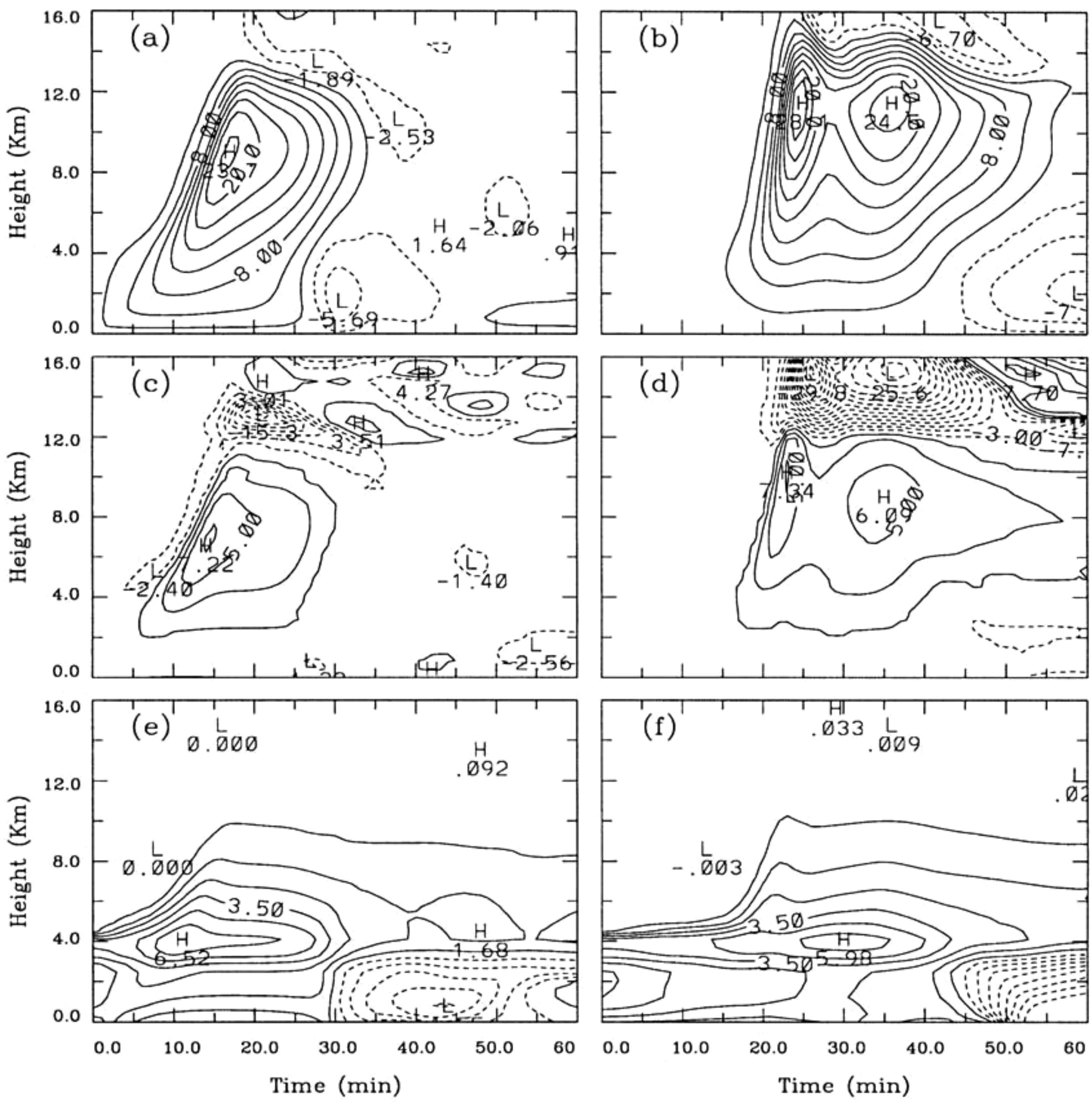

Figure 18. Time evolutions of the (a) vertical velocity (ms^{-1}), (c) potential temperature anomaly (K), and (e) moisture anomaly (kg kg^{-1}) from the one-dimensional cloud model, and the averaged (b) vertical velocity (m s^{-1}), (d) potential temperature anomaly (K), and (f) moisture anomaly (kg kg^{-1}) within the radius of 5000 m cloud from the WRF model. The values in (e) and (f) are multiplied by 1×103 (Chen and Sun, 2002).

(b) applying a spatial filter to remove the unwanted shortwaves and the values beyond the constraints, and finally (c) introducing a polynomial or sine function as the correction function that conserves mass, while inducing the least modification to the results obtained from (a) and (b). Numerical simulations of pure advection, rotation, and idealized cyclogenesis show that the scheme is very accurate compared with analytic solutions, as shown in Fig. 19 (Sun and Sun, 2004). With the variational techniques, this scheme is capable of reproducing the positive-definite results and conservation of total mass and total energy in the shallow water equations in both rotational and irrotational frames (Sun, 2007).

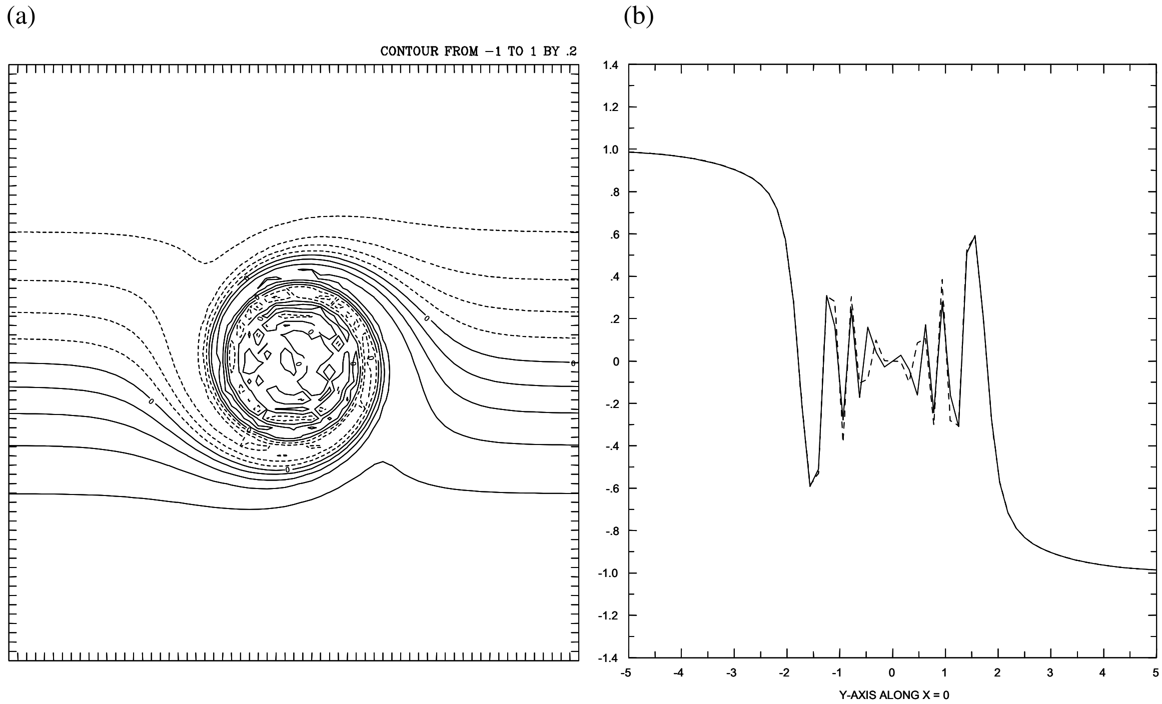

Figure 19. (a) Horizontal plane of numerical simulation and (b) vertical profiles of analytic solution (dashed line) and numerical result (solid line) of Doswell's idealized cyclogenesis after 16 time steps with courant number = 4.243, revolution = 4.386 and δ (transition width) = 2.0 with mass correction but without internet filter (Sun and Sun, 2004).

4.7. *2D shallow water equations*

Oh (2007) applied the semi-Lagrangian integration method (Sun *et al.*, 1996; Sun and Yeh, 1997) combined with the method of characteristics to the 2D shallow water equations to study the geostrophic adjustment problem, the shear instability, the collapse of a circular dam, the interaction of a vortex with the terrain, and the merging of vortices. His results show that the scheme is highly accurate in simulating flows involving a sharp gradient, such as the collapse of the cylindrical dam and the merging of two vortices. The characteristic approach is easier to interpret. Figure 20(a) shows the height at different times, and Fig. 20(b) the PV (potential vorticity), revealing that the height (or kinetic energy) cascades to the larger wavelength while the vorticity field cascades to the smaller wavelength in a 2D flow.

5. Summary

For the past several decades, numerical models have substantially improved in simulating short-term weather and long-term climate change. However, tremendous work is still required to improve the basic equations, numerical methods, resolvable and subgrid scale physical parametrizations, and initial and boundary conditions (Sun, 2002). More observational data is also required to provide better initial and boundary conditions. The reanalysis data, which has been used for initial and boundary conditions in weather/climate simulations, is a combination of model output and observations. More observations are also needed to validate the model results. Finally, we need better computational resources (both hardware and software) in order to develop new models with finer resolution and comprehensive

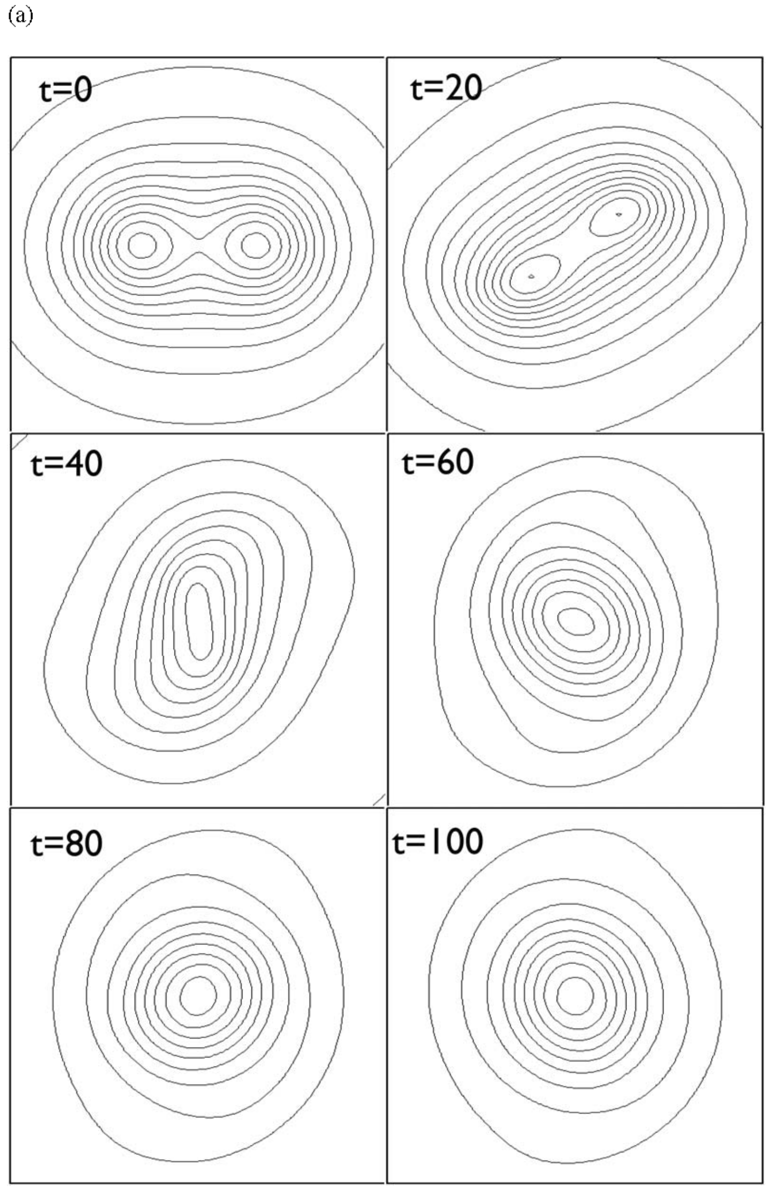

Figure 20. Simulated (a) height field and (b) potential vorticity of a merger of two vortices. Results are shown in 20 s time intervals.

physics/parametrizations, as well as to display model results.

Numerical modeling is an exciting and challenging field. With the appropriate equations, numerical methods, and initial and boundary conditions, the models can reveal the spatial and temporal evolution of the processes involved. Models can also be used to simulate climate/environment in the past or in the future, which cannot be carried out in the laboratory or in field experiments. Hence, numerical models are the most important tool in weather forecasting and climate study. However, we should also be aware that uncertainty

(b)

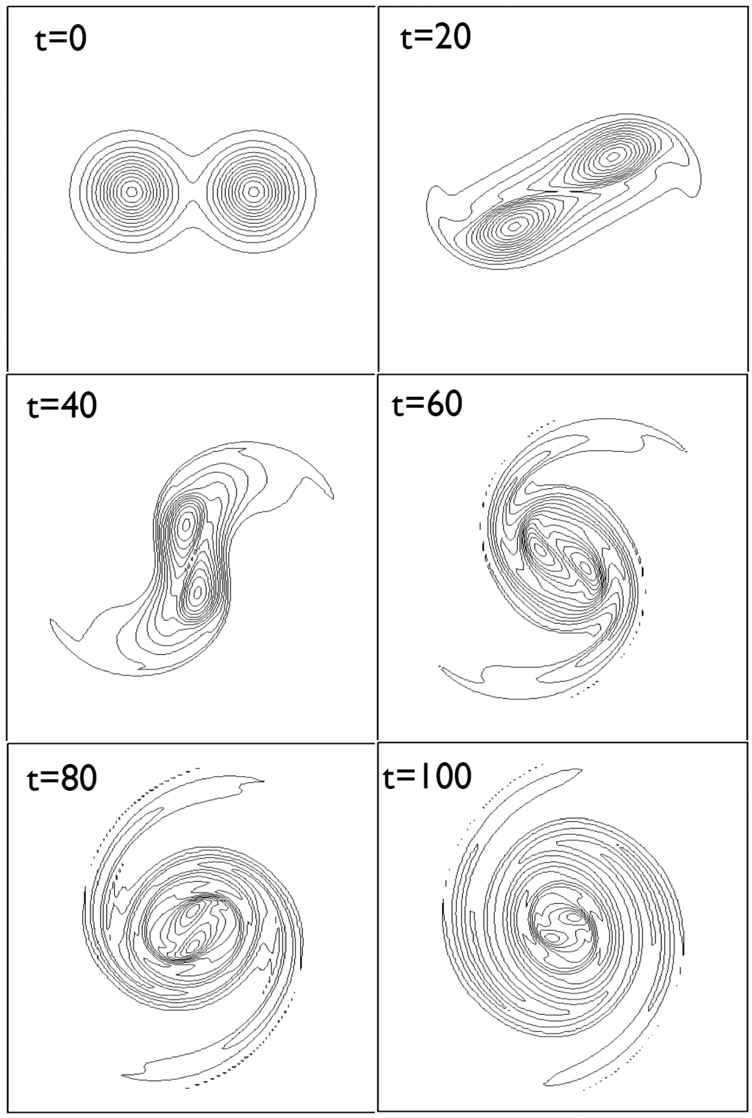

Figure 20. (*Continued*)

always exists in weather/climate models, which can be caused by errors in equations, physical parametrizations, resolution, initial and boundary conditions, numerical methods, etc. (Sun, 2006a,b).

[Received 19 January 2007; Revised 19 October 2007; Accepted 23 October 2007.]

References

Anthes, R. A., 1977: A cumulus parameterization scheme utilizing a one-dimensional cloud model. *Mon. Wea. Rev.*, **105**, 270–286.

Bosilovich, M. G., and W. Y. Sun, 1995: Formation and verification of a land surface parameterization for atmospheric models. *Boundary-Layer Meteor.*, **73**, 321–341.

Bosilovich, M. B., and W. Y. Sun, 1998: Monthly simulation of surface layer fluxes and soil properties during FIFE. *J. Atmos. Sci.*, **55**, 1170–1183.

Bosilovich, M. G., and W. Y. Sun, 1999a: Numerical simulation of the 1993 Midwestern flood: local and remote sources of water. *J. Geophys. Res.*, **104**, D1, 19415–19423.

Bosilovich, M. G., and W. Y. Sun, 1999b: Numerical simulation of the 1993 Midwestern flood: land–atmosphere interactions. *J. Climate*, **12**, 1490–1505.

Carter, W. P. L., J. A. Pierce, D. Luo, and I. L. Malkina, 1995: Environmental chamber studies of maximum incremental reactivities of volatile organic compounds. *Atmos. Environ.*, **29**, 2499–2511.

Carter, W. P. L., D. Lu, and I. L. Malkina, 1997: Environmental chamber studies for development of an updated photochemical mechanism for VOC reactivity assessment. Draft final report to California Air Resources Board Contract 92–345, Coordinating Research Council Project M-9, and National Renewable Energy Laboratory Contract ZF-2–12252-07.

Caughey, S. J., and S. G. Palmer, 1979: Some aspects of turbulence structure through the depth of convective layer. *Quart. J. Roy. Meteor. Soc.*, **105**, 811–827.

Chen, S. H., and W. Y. Sun, 2001: The applications of the multigrid method and a flexible hybrid coordinate in a nonhydrostatic model. *Mon. Wea. Rev.*, **129**, 2660–2676.

Chen, S. H., and W. Y. Sun, 2002: A one-dimensional time dependent cloud model. *J. Meteor. Soc. Japan*, **80**, 99–118.

Chen, S. H., and W. Y. Sun, 2004: An explicit one-dimensional time-dependent tilting cloud model. *J. Atmos. Sci.*, **61**, 2797–2816.

Chen, Y. L., and N. B. F. Hui, 1990: Analysis of a shallow front during the Taiwan Area Mesoscale Experiment. *Mon. Wea. Rev.*, **118**, 2649–2667.

Chen, T.-C., W.-R Huang, and W. A. Gallus Jr., 2002: An East Asian cold surge: case study. *Mon. Wea. Rev.*, **130**, 2271–2290.

Chern, J. D., 1994: Numerical simulation of cyclogenesis over the western United States. PhD thesis (Department of Earth and Atmospheric Sciences, Purdue University, W. Lafayette, IN, USA), pp. 178.

Chern, J. D., and W. Y. Sun, 1998: Formulation and validation of a snow model. A11A-06, 1998 Fall Meeting, AGU, supplement to EOS, AGU, 79, 45. F96. 10 Nov. 1998.

Chou, M. D., and M. J. Suarez, 1994: An efficient thermal infrared radiation parameterization for use in general circulation models. NASA Tech. Memo. 104606, Vol. 3, pp. 85.

Chou, M. D., M. J. Suarez, X.-Z. Liang, and M. M.-H. Yan, 2001: A thermal infrared radiation parameterization for atmospheric studies. NASA/TM-2001-104606, NASA GSFC, Greenbelt USA, MD, USA.

Crowley, W. P., 1969: Numerical advection experiment. *Mon. Wea. Rev.*, **96**, 1–11.

Deardorff, J. W., and G. E. Willis, 1975: A parameterization of diffusion into mixed layer. *J. Appl. Meteor.*, **14**, 1451–1458.

DeFries, R. S., and J. R. G. Townshend, 1994: NDVI-derived land cover classification a global scale. *Int. J. Remote Sens.*, **15**, 3567–3586.

Doswell, C. A., III, 1984: A kinematic analysis associated with a nondivergent vortex. *J. Atmos. Sci.*, **41**, 1242–1248.

Gill, A. E., 1982: *Atmosphere–Ocean Dynamics.* (Academic, New York), pp. 662.

Ginoux, P., M. Chin, I. Tegen, J. M. Prospero, B. Holben, O. Dubovik, and S.-J. Lin, 2001: Sources and distributions of dust aerosols simulated with the GOCART model. *J. Geophys. Res.*, **106**, D17, 20255–20273.

Grell, G. A., J. Dudhia, and D. R. Stauffer, 1995: A description of the fifth-generation Penn State/NCAR mesoscale model (MM5). NCAR/TN-398 + STR, (National Center for Atmospheric Research, Boulder, CO, USA), pp. 122.

Haines, A. P., and W. Y. Sun, 1994: A convective cloud model for use in a cumulus parameterization scheme. *Mon. Wea. Rev.*, **122**, 165–182.

Haines, P. A., J. D. Chern, and W. Y. Sun, 1997: Numerical simulation of the Valentine's Day storm during WISP 1990. *Tellus*, **49A**, 595–612.

Haines, P. A., D. J. Grove, W. Y. Sun, W. R. Hsu, and S. C. Tcheng, 2003: High resolution results and scalability of numerical modeling of wind flow at White Sand missile range. BACIMO (DOD atmospheric science and effects) conference (Sept. 2003, Monterey, California).

Hsu, K. J., 2001: Numerical simulations of local atmospheric circulation and pollution tracks in northern Taiwan. Taipei County Environment Protection Bureau Report, 235 pp.

Hsu, H. H., Y. C. Yu, W. S. Kau, W. R. Hsu, and W. Y. Sun, 2004: Simulation of the 1998 East Asian summer monsoon using Purdue regional model. *J. Meteor. Soc. Japan*, **82**, 1715–1733.

Hsu, H. H., W. R. Hsu, W. S. Kau, Y. C. Yu, and W. Y. Sun, 2003: Simulation of the 1998

East Asian Summer Monsoon using Purdue Regional Climate Model. The Second Workshop on Regional Climate Modeling for Monsoon System. (Mar. 4–6, 2003; Yokohama, Japan).

Hsu, W. R., and W. Y. Sun, 1991: Numerical study of mesoscale cellular convection. *Boundary-Layer Meteor.*, **57**, 167–186.

Hsu, W. R., and W. Y. Sun, 1994: A numerical study of a low-level jet and its accompanying secondary circulation in a Mei-yu system. *Mon. Wea. Rev.*, **122**, 324–340.

Hsu, W. R., and W. Y. Sun, 2001: A time-split, forward–backward numerical model for solving a nonhydrostatic and compressible system of equations. *Tellus*, **53A**, 279–299.

Hsu, W. R., W. Y. Sun, S. C. Tcheng, and H. Y. Chang, 2000: Parallel of the NTU–Purdue nonhydrostatic numerical model: simulation of the 11 January 1972 Boulder windstorm. The Seventh National Computational Fluid Dynamics Conference. (Aug. 2000, Kenting, Taiwan).

Hsu, W. R., J. P. Hou, C. C. Wu, and W. Y. Sun, 2004: Large-eddy simulation of cloud streets over the East China Sea during cold-air outbreak events. 16th Symposium on Boundary Layer and Turbulence, (Aug. 9–13, 2004; Portland, Maine, USA).

Kuo, H. L., 1949: Dynamically instability of two-dimensional nondivergent flow in a barotropic atmosphere. *J. Meteor.*, **6**, 105–122.

Kuo, H. L., 1963: Perturbations of plane Couetter flow. I: A stratified fluid and origin of cloud streets. *Phys. Fluid*, **6**, 195–211.

Kuo, H. L., 1965: On formation and intensification of tropical cyclones through latent heat release by cumulus convection. *J. Atmos. Sci.*, **22**, 40–63.

Kuo, H. L., 1974: Further studies of the parameterization of the influence of cumulus convection on large-scale flow. *J. Atmos. Sci.*, **31**, 1232–1240.

Kuo, Y. H., and G. T. J. Chen, 1990: Taiwan Area Mesoscale Experiment: an overview. *Bull. Amer. Meteor. Soc.*, **71**, 488–503.

Lin, Y.-L., R. D. Farley, and H. D. Orville, 1983: Bulk parameterization of the snow field in a cloud model. *J. Climate Appl. Meteor.*, **22**, 1065–1092.

Lilly, D. K., 1978: A severe downslope windstorm and aircraft turbulence event induced by a mountain wave. *J. Atmos. Sci.*, **35**, 59–77.

Liou, K. N, Q. Fu, and T. P. Ackerman, 1988: A simple formulation of the delta-four-stream approximation for radiative transfer parameterizations. *J. Atmos. Sci.*, **45**, 1940–1947.

MacCall, B. T., 2006: Application of Reynolds' stress closure to the stable boundary layer. PhD thesis, Department Earth and Atmospheric Sciences, Purdue University, W. Lafayette, IN USA.

Malkus, J. S., and H. Riehl, 1964: *Cloud Structure and Distribution over the Tropical Pacific Ocean* (University of California Press, Berkeley, Los Angeles), pp. 229.

Marticorena, B., and G. Bergametti, 1995: Modeling the atmospheric dust cycle. I: Design of a soil-derived dust emission scheme. *J. Geophys. Res.*, **100**(D8), 16415–16430.

Min, K.-H., 2005: Coupled cryosphere model development for regional climate study and the initialization of Purdue Regional Model with the land data assimilation system. PhD thesis (Department Earth and Atmospheric Sciences, Purdue University, W. Lafayette, IN, USA) pp. 149.

Molinari, J., 1982: A method for calculating the effects of deep cumulus convection in numerical models. *Mon. Wea. Rev.*, **110**, 1527–1534.

Oglesby, R. J., and D. Erikson, 1989: Soil moisture and persistence of North American drought. *J. Climate*, **2**, 1362–1380.

Oglesby, R. J., 1991: Springtime soil moisture, natural climatic variability and North American drought as simulated by the NCAR Community Climate Model 1. *J. Climate*, **4**, 890–897.

Oh, T.-J., 2003: Numerical study of flow past an idealized bell shape mountain with varying Froude number. MS thesis (Department of Earth and Atmospheric Sciences, Purdue University, W. Lafayette, IN, USA) pp. 106.

Oh, T.-J., 2007: Development and testing of characteristic-based semi-Lagrangian two-dimensional shallow water equations development and testing of characteristic-based semi-Lagrangian two-dimensional shallow water equations model. PhD thesis, department of Earth and Atmospheric Sciences, Purdue University, W. Lafayette, IN, USA.

Queney, P., 1948: The problem of airflow over mountains: a summary of theoretical studies. *Bull. Amer. Meteor. Soc.*, **29**, 16–26.

Schaefer, J. T., 1974: The life cycle of the dryline. *J. Appl. Meteor.*, **13**, 444–449.

Scorer, R. S., 1949: Theory of waves in the lee of mountains. *Quart. J. Roy. Meteor. Soc.*, **75**, 41–56.

Skamarock, W., J. Klemp, J. Dudhia, D. Gill, D. Barker, W. Wang, and J. Powers, 2005:

A description of the Advanced Research WRF version 2. NCAR technical note, 100 pp.

Smith, R. B., 1979: The influence of mountains on the atmosphere. In *Advances in Geophysics*, Vol. 21 ed. B. Saltzman, (Academic), pp. 87–230.

Smith, R. B., 1980: Linear theory of stratified hydrostatic flow past an isolated mountain. *Tellus*, **32**, 348–364.

Smolarkiewicz P. K., and R. Rotunno., 1989: Low Froude number flow past three-dimensional obstacles. Part I: Baroclinically generated Lee vortices. *J. Atmos. Sci.*, **46**, 1154–1164.

Sun, W. Y., 1978: Stability of deep cloud streets. *J. Atmos. Sci.*, **35**, 466–483.

Sun, W. Y., 1980: A forward–backward time integration scheme to treat internal gravity waves. *Mon. Wea. Rev.*, **108**, 402–407.

Sun, W. Y., 1982: A comparison of two explicit time integration schemes applied to the transient heat equation. *Mon. Wea. Rev.*, **110**, 1645–1652.

Sun, W. Y., 1984a: Numerical analysis for hydrostatic and nonhydrostatic equations of inertial–internal gravity waves. *Mon. Wea. Rev.*, **112**, 259–268.

Sun, W. Y., 1984b: Rainbands and symmetric instability. *J. Atmos. Sci.*, **41**, 3412–3426.

Sun, W. Y., 1984c: Pollution in the atmosphere. *NATPA Bull.*, **4**, 30–32.

Sun, W. Y., 1986: Air pollution in a convective boundary. *Atmos. Environ.*, **20**, 1877–1886.

Sun, W. Y., 1987: Mesoscale convection along the dryline. *J. Atmos. Sci.*, **44**, 1394–1403.

Sun, W. Y., 1988: Air pollution in a convective atmosphere. In *Library of Environmental Control Technology* ed. Cheremisinoff (Gulf), pp. 515–546.

Sun, W. Y., 1989: Diffusion modeling in a convective boundary layer. *Atmos. Environ.*, **23**, 1205–1217.

Sun, W. Y., 1990a: Modified Eady waves and frontogenesis. Part I: Linear stability analysis. *Terrestrial, Atmospheric and Oceanic Sciences*, **1**, 363–378.

Sun, W. Y., 1990b: Modified Eady waves and frontogenesis. Part II: Nonlinear Integration. *Terrestrial, Atmospheric and Oceanic Sciences*, **1**, 379–392.

Sun, W. Y., 1993a: Numerical simulation of a planetary boundary layer. Part I. Cloud-free case. *Beitr. Phys. Atmos.*, **66**, 3–16.

Sun, W. Y., 1993b: Numerical simulation of a planetary boundary layer. Part II. Cloudy case. *Beitr. Phys. Atmos.*, **66**, 17–30.

Sun, W. Y., 1993c: Numerical experiments for advection equation. *J. Comput. Phys.*, **108**, 264–271.

Sun, W. Y., 1995a: Pressure gradient in a sigma coordinate. *Terrestrial, Atmospheric and Oceanic Sciences*, **4**, 579–590.

Sun, W. Y., 1995b: Unsymmetrical symmetric instability. *Quart. J. Roy. Meteor. Soc.*, **121**, 419–431.

Sun, W. Y., 2002: Numerical modeling in the atmosphere. *J. Korean Meteorol. Soc.*, **38**, 3, 237–251.

Sun, W. Y., 2006a: Uncertainties in climate models (To appear in 10th edition of *McGraw-Hill Encyclopedia of Sciences & Technology*).

Sun, W. Y., 2006b: Regional climate modeling. In *McGraw-Hill 2006 Yearbook of Science & Technology*.

Sun, W. Y., 2007: Conserved semi-Lagrangian scheme applied to one-dimensional shallow water equations. *Terrestrial, Atmospheric and Oceanic Science*, **18**, 777–803.

Sun, W. Y., and M. G. Bosilovich, 1996: Planetary boundary layer and surface layer sensitivity to land surface parameters. *Boundary-Layer Meteor.*, **77**, 353–378.

Sun, W. Y., and C. Z. Chang, 1986a: Diffusion model for a convective layer. Part 1: Numerical simulation of a convective boundary layer. *J. Climate Appl. Meteor.*, **25**, 1445–1453.

Sun, W. Y., and C. Z. Chang, 1986b: Diffusion model for a convective layer. Part II: Plume released from a continuous point source. *J. Climate Appl. Meteor.*, **25**, 1454–1463.

Sun, W. Y., and Y. L. Chang, 1992: Barotropic instability of the modified hyper-tangent shear flows. *Beitr. Phys. Atmos.* **65**, 193–210.

Sun, W. Y., and J. D. Chern, 1993: Diurnal variation of lee-vortexes in Taiwan and surrounding area. *J. Atmos. Sci.*, **50**, 3404–3430.

Sun, W. Y., and J. D. Chern, 1994: Numerical experiments of vortices in the wake of idealized large mountains. *J. Atmos. Sci.*, **51**, 191–209.

Sun, W. Y., and J. D. Chern, 1998: Air-sea-ice model applied in the Arctic region. A72D-06, 1998 Fall Meeting, AGU, supplement to EOS, AGU, 79, 45. F94. 10 Nov. 1998.

Sun, W. Y., and J. D. Chern, 1999: Numerical simulation of southeast Asia weather in May–June of 1998. Preprint, Workshop on Regional Climate (11 Mar 1999; The Center of Ocean Research, National Taiwan University, Taipei, Taiwan) p. 12.

Sun, W. Y., and J. D. Chern, 2005: One-dimensional snow-land surface model applied to

Sleepers experiment. *Boundary-Layer Meteor.*, **116**, 95–115.

Sun, W. Y., and J. D. Chern, 2006: A numerical study of influence of central mountain ranges on a cold front. *J. Meteorol. Soc. Japan*, **84**, 27–46.

Sun, W. Y., and P. A. Haines, 1996: Semi-prognostic tests of a new mesoscale cumulus parameterization scheme. *Tellus*, **48A**, 272–289.

Sun, W. Y., and W. R. Hsu, 1988: Numerical study of cold air outbreak over the warm ocean. *J. Atmos. Sci.*, **45**, 1205–1227.

Sun, W. Y., and W. R. Hsu, 2005: Effect of surface friction on downslope wind and mountain waves. *Terrestrial, Atmospheric and Oceanic Science*, **16**, 393–418.

Sun, W. Y., and Y. Ogura, 1980: Modeling the evolution of the convective planetary boundary layer. *J. Atmos. Sci.*, **37**, 1558–1572.

Sun, W. Y., and Y. Ogura, 1979: Boundary-layer forcing as a possible trigger to a squall-line formation. *J. Atmos. Sci.*, **36**, 235–254.

Sun, W. Y., and I. Orlanski, 1981a: Large mesoscale convection and sea breeze circulation. Part I: linear stability analysis. *J. Atmos. Sci.*, **38**, 1675–1693.

Sun, W. Y., and I. Orlanski, 1981b: Large mesoscale convection and sea breeze circulation. Part 2: Non-linear numerical model. *J. Atmos. Sci.*, **38**, 1694–1706.

Sun, W. Y., and M. T. Sun, 2004: Mass correction applied to semi-Lagrangian advection scheme. *Mon. Wea. Rev.*, **132**, 975–984.

Sun, W. Y., and R. Y. Sun, 2004: Relationship between canopy and climate chap. 2 of *Protected Horticulture Science*, ed. C. Tsay (Research Institute of Agriculture, Taiwan), pp. 11–31.

Sun, W. Y., and C. C. Wu, 1992: Formation and diurnal oscillation of dryline. *J. Atmos. Sci.*, **49**, 1606–1619.

Sun, W. Y., and K. S. Yeh., 1997: A general semi-Lagrangian advection scheme employing forward trajectories. *Quart. J. Roy. Meteor. Soc.*, **123**, 2463–2476.

Sun, W. Y., and A. Yildirim, 1989: Air mass modification over Lake Michigan. *Boundary-Layer Meteor.*, **48**, 345–360.

Sun, W. Y., J. D. Chern, C. C. Wu, and W. R. Hsu, 1991: Numerical simulation of mesoscale circulation in Taiwan and surrounding area. *Mon. Wea. Rev.*, **119**, 2558–2573.

Sun, W. Y., W. R. Hsu, and J. D. Chern, 1995: Numerical simulation of an active Mei-yu front. International Workshop on Heavy Rainfall in East Asia, (27–29 Seoul, South Korea, Mar. 1995), pp. 108–113.

Sun, W. Y., K. S. Yeh, and R. Y. Sun, 1996: A simple semi-Lagrangian scheme for advection equation. *Quart. J. Roy. Meteor. Soc.*, **122**, 1211–1226.

Sun, W. Y., M. G. Bosilovich, and J. D. Chern, 1997: CCM1 regional response to anomalous surface properties. *Terrestrial, Atmospheric and Oceanic Sciences*, **8**, 271–288.

Sun, W. Y., J. D. Chern, and M. Bosilovich, 2004: Numerical study of the 1988 drought in the United States. *J. Meteorol. Soc. Japan*, **82**, 1667–1678.

Tegen, I., and I. Fung, 1994: Modeling of mineral dust in the atmosphere: sources, transport, and optical thickness. *J. Geophys. Res.*, **99**(D11), 22897–22914.

Weisman, M. L, and J. B. Klemp, 1984: The structure and classification of numerically simulated convective storms in directionally varying wind shears. *Mon. Wea. Rev.*, **112**, 2479–2498.

Willis, G. E., and J. W. Deardorff, 1978: A laboratory study of dispersion from an elevated source within a modeled convective planetary boundary layer. *Atmos. Environ.*, **12**, 1305–1311.

Willis, G. E., and J. W. Deardorff, 1981: A laboratory study of dispersion from a source in the middle of the convective planetary boundary layer. *Atmos. Environ.*, **15**, 109–117.

Wu, C.-C., and W. Y. Sun, 1990a: Diurnal oscillation of convective boundary layer. Part I: Cloud-free atmosphere. *Terrestrial, Atmospheric and Oceanic Sciences*, **1**, 23–43.

Wu, C.-C., and W. Y. Sun, 1990b: Diurnal oscillation of convective boundary layer. Part II: Cloudy atmosphere. *Terrestrial, Atmospheric and Oceanic Sciences*, **2**, 157–174.

Wu, C. C., Y. C. Yu, W. R. Hsu, K. J. Hsu, and W. Y. Sun, 2003: Numerical study on the wind fields and atmospheric transports of a typical winter case in Taiwan and surrounding area. *Atmos. Sci.*, **31**, 29–54 (in Chinese).

Yang, K. J.-S., 2004a: Numerical simulations of Asian aerosols and their regional climatic impacts: dust storms and bio-mass burning. MS thesis, (Department of Earth and Atmospheric Sciences, Purdue University, W. Lafayette, IN, USA), pp. 141.

Yang, K. J.-S., 2004b: Regional climate-chemistry model simulations of ozone in the lower troposphere and its climatic impacts. PhD thesis, (School of Civil Engineering, Purdue University, W. Lafayette, IN, USA), pp. 157.

Yildirim, A., 1994: Numerical study of an idealized cyclone evolution and its sub-synoptic features. PhD thesis (Department of Earth and Atmospheric Sciences, Purdue University, W. Lafayette, IN USA), pp. 145.

Yu, Y. C., H. H. Hsu, W. S. Kau, T. H. Tsou, W. R. Hsu, and W. Y. Sun, 2004a: An evaluation of the East Asian summer monsoon simulation by the Purdue Regional Model . *J. Environ. Protect Soc. Taiwan*, **27**, 41–56.

Yu, Y. C., H.-H. Hsu, W. S. Kau, T. H. Tsou, W. R. Hsu, W. Y. Sun, and W. N. Yu, 2004b: An evaluation of the east Asian summer monsoon simulation using the Purdue Regional Model. Third Workshop on Regional Climate Modeling for Monsoon System (Hawaii, 17 Feb. 2004).